



# Integrated Arctic Observation System

Research and Innovation Action under EC Horizon2020  
Grant Agreement no. 727890

Project coordinator:  
Nansen Environmental and Remote Sensing Center, Norway


## Deliverable 3.15

**Final implementation of the observing system:  
Data delivery and report on results  
of the distributed systems for atmosphere and land**

Start date of project:	01 December 2016	Duration:	60 months
Due date of deliverable:	31 May 2021	Actual submission date:	12 July 2021
Lead beneficiary for preparing the deliverable:	MPG		
Person-months used to produce deliverable:	66.97 pm		

Authors: Mathias Göckede, Florent Domine, Walter Oechel, Roberta Pirazzini, Torsten Sachs, Michael Tjernström, Donatella Zona

Version	DATE	CHANGE RECORDS	LEAD AUTHOR
1.0	14.10.2019	Template	A. Beszczynska-Möller
1.1	30.06.2021	1 <sup>st</sup> Draft, submitted for internal review	M. Göckede
1.2	08.07.2021	Reviewed	A. Beszczynska-Möller
1.3	12.07.2021	Final version, submitted for publication	M. Göckede

<b>Approval</b>	Date: 12 July 2021	Sign.  Stein Sandven
-----------------	--------------------	---

USED PERSON-MONTHS FOR THIS DELIVERABLE					
No	Beneficiary	PM	No	Beneficiary	PM
17	MPG	17.5			
30	GFZ	6			
48	UNEXE	10			
14	USFD	4			
28	CNRS-Takuvik	12			
10	FMI	5.47			
4	MISU	12			

DISSEMINATION LEVEL		
PU	Public, fully open	X
CO	Confidential, restricted under conditions set out in Model Grant Agreement	
CI	Classified, information as referred to in Commission Decision 2001/844/EC	

**EXECUTIVE SUMMARY**

This document, ***Deliverable 3.15 - Final implementation of the observing system: Data delivery and report on results of the distributed observing systems for atmosphere and land***, describes the work conducted within INTAROS WP3.5. This WP comprises contributions from seven different partners, operating novel terrestrial or atmospheric observations across different methodological and geographical areas in the Arctic.

This document is intended to:

- Demonstrate that all partners delivered their results/products according to the requirements listed in the description of work;
- Summarize changes in the work plan in the context of COVID-19 related problems, mostly linked to travel restrictions and inaccessibility of field sites. These issues reduced the findings that can be reported here, however, without substantially compromising the overarching objectives;
- Describe, on a activity-by-activity level, the novel observations implemented by each partner, the datasets obtained, and their suitability for continuous, long-term operations in an improved future Arctic observing system;
- Document the ‘lessons learned’ while designing, installing and operating the novel observation techniques;
- Provide a concise interpretation of the specific datasets that were obtained within WP3.5 observational campaigns;
- Summarize data availability, including links to publicly accessible repositories where data can be retrieved by the scientific community;
- Give an outlook on plans and options regarding the future operation of the specific observation systems.

## Table of Contents

1.	Introduction .....	5
2.	Final implementation and operational use of the distributed observing systems for ocean and sea ice.....	7
2.1.	MPG.....	7
2.1.1.	Results of the final implementation of the observing system.....	7
2.1.2.	Lessons learned and technology challenges identified during the project.....	8
2.1.3.	Description of processing and analysis of the obtained data .....	9
2.1.4.	Accessibility of the obtained data sets and repositories used.....	12
2.1.5.	Future plans for operation of the observing system, including data provision	12
2.2.	GFZ .....	13
2.2.1.	Results of the final implementation of the observing system .....	13
2.2.2.	Lessons learned and technology challenges identified during the project.....	14
2.2.3.	Description of processing and analysis of the obtained data .....	14
2.2.4.	Accessibility of the obtained data sets and repositories used.....	14
2.2.5.	Future plans for operation of the observing system, including data provision	14
2.3.	UNEXE.....	14
2.3.1.	Results of the final implementation of the observing system .....	14
2.3.2.	Lessons learned and technology challenges identified during the project.....	15
2.3.3.	Description of processing and analysis of the obtained data .....	15
2.3.4.	Accessibility of the obtained data sets and repositories used.....	16
2.3.5.	Future plans for operation of the observing system, including data provision	17
2.4.	USFD .....	17
2.4.1.	Results of the final implementation of the observing system .....	17
2.4.2.	Lessons learned and technology challenges identified during the project.....	17
2.4.3.	Description of processing and analysis of the obtained data .....	19
2.4.4.	Accessibility of the obtained data sets and repositories used.....	19
2.4.5.	Future plans for operation of the observing system, including data provision	20

2.5.	CNRS-Takuvik.....	20
2.5.1.	Results of the final implementation of the observing system .....	20
2.5.2.	Lessons learned and technology challenges identified during the project.....	23
2.5.3.	Description of processing and analysis of the obtained data .....	24
2.5.4.	Accessibility of the obtained data sets and repositories used.....	24
2.5.5.	Future plans for operation of the observing system, including data provision 24	
2.6.	FMI .....	25
2.6.1.	Results of the final implementation of the observing system .....	25
2.6.2.	Lessons learned and technology challenges identified during the project.....	28
2.6.3.	Description of processing and analysis of the obtained data .....	29
2.6.4.	Accessibility of the obtained data sets and repositories used.....	32
2.6.5.	Future plans for operation of the observing system, including data provision 32	
2.7.	MISU .....	33
2.7.1.	Results of the final implementation of the observing system .....	34
2.7.2.	Lessons learned and technology challenges identified during the project.....	37
2.7.3.	Description of processing and analysis of the obtained data .....	38
2.7.4.	Accessibility of the obtained data sets and repositories used.....	42
2.7.5.	Future plans for operation of the observing system, including data provision 42	
3.	Performance and fitness-to-purpose of the platforms, sensors and systems implemented during INTAROS for a future sustained Arctic observing system .....	43
4.	Summary .....	45
5.	Literature.....	46

## 1. Introduction

INTAROS WP3 focused on developing and implementing innovative solutions and new technologies to fill selected gaps identified in the existing Arctic observing systems. Novel instruments and sampling methods were further integrated with mature components of

existing observatories to increase temporal and geographic coverage of in situ observational data in the Arctic. INTAROS partners involved in Task 3.5, which provides the input for this report, covered multi-disciplinary observations summarized as a distributed observatory for terrestrial and atmospheric components.

As a distributed system covering different spheres of the Arctic, research activities within Task 3.5 were highly diverse regarding area of implementation (see also Figure 1), spatio-temporal scales covered, and observation techniques employed. As a short overview, the following list highlights activities by seven INTAROS partners that contributed to this report:

1. MPG: Operation of an automated flask sampler for atmospheric trace gases (Greenland)
2. GFZ: Re-processing and uniform formatting of existing databases of vertical aircraft profiles of atmospheric boundary layer state variables (multiple Arctic locations).
3. UNEXE: Winter-proofing eddy-covariance instrumentation (Alaska).
4. USFD: High-resolution vertical soil profiles of temperature and gas concentrations (Alaska).
5. CNRS-Takuvik: Multi-disciplinary monitoring of snow and vegetation properties (Canada).
6. FMI: Improved ground-truthing of satellite remote sensing products (Finland).
7. MISU: Icebreaker-based multi-disciplinary monitoring of atmospheric properties (Arctic Ocean).

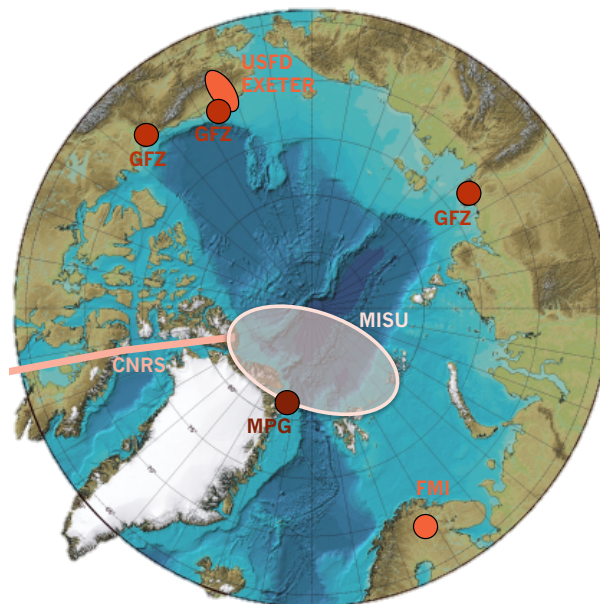


*Figure 1: Overview on locations covered by the seven novel observation campaigns summarized in this report.*

Without a substantial geographical or methodological overlap, the research programs comprised within this report cannot be combined towards addressing an overarching scientific objective. However, all of them fill crucial gaps in the previously existing Arctic monitoring capacity. As such, the new devices jointly contribute to strengthen the integrated scientific insights into the terrestrial and atmospheric spheres within the

Arctic. The individual reports provided in the following Section 2 summarize the details on implementation and operation of each system, including an overview on collected datasets and their availability.

## 2. Final implementation and operational use of the distributed observing systems for ocean and sea ice

### 2.1. MPG

Contributors: Mathias Göckede, Martijn Pallandt, Richard Kneißl, Markus Erritt

#### 2.1.1. Results of the final implementation of the observing system

MPG installed and operated a flask sampler that can be used for the automated collection of air samples under standardized conditions at remote Arctic sites. In their full-sized version, these samplers developed by the ICOS-FCL laboratory consist of five drawers (see e.g. Figure 2, left panel), as described in more detail in Levin et al. (2020). The sampler version used by MPG is smaller compared to the one shown in Figure 2, consisting of just 3 drawers., one of which is reserved for pumps, computers, etc. The other two drawers reserved for the samples have a combined holding capacity up to 12 flasks at a time. The right panel of Figure 2 shows an example of the flow scheme monitoring tool, indicating the states of all integrated valves, pumps, flask ports, sensors and mass flow controllers.

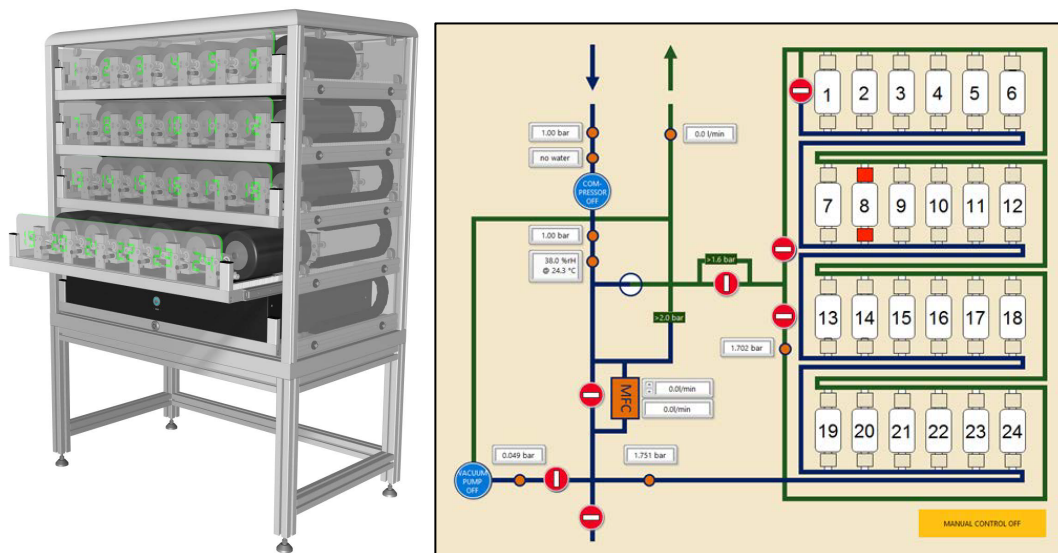


Figure 2: (left) Front view of a 24-port flask sampler. (right) control panel showing the flow scheme within a 24-port sampler.

Flasks were analyzed at MPI-BGC in Jena for the concentrations of CH<sub>4</sub>, CO<sub>2</sub>, CO, N<sub>2</sub>O, H<sub>2</sub>, and SF<sub>6</sub>. As additional parameters, we sampled the ratios of O<sub>2</sub>/N<sub>2</sub>, Ar/N<sub>2</sub>, and the stable isotope signals d<sup>13</sup>C-CO<sub>2</sub>, d<sup>18</sup>O-CO<sub>2</sub>, d<sup>13</sup>C-CH<sub>4</sub>, and d<sup>2</sup>H-CH<sub>4</sub>. The sampler facilitates multiple modes for filling flasks. For our Arctic deployment, we chose three different strategies:

1. A fraction of the samples was filled according to a fixed, user-prescribed schedule.

2. Other flasks were reserved to be filled based on external triggers, e.g. a high-concentration event of atmospheric methane, or CO<sub>2</sub>.
3. The last fraction was used for slow filling of multiple flasks over a longer timeframe, where specific flasks were selected for five different regions of origin of the air masses sampled.

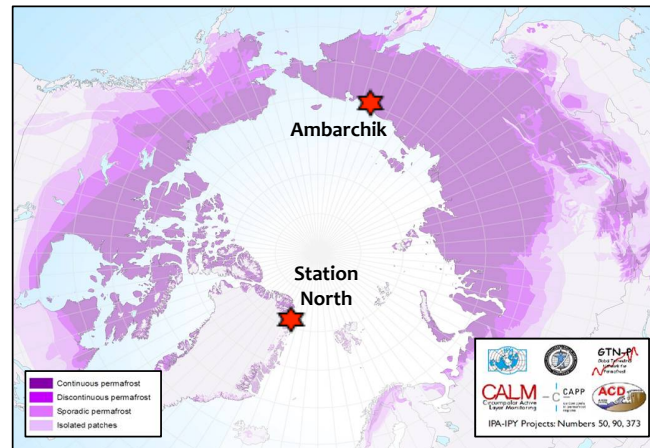


Figure 3: Locations of flask sampler deployment. See main text for more details.

Installation of the instrument was originally planned for the site Ambarchik in Northeast Siberia (see also Figure 3). Due to unexpected delays linked to customs problems in 2019, the installation schedule was seriously jeopardized, therefore we developed an alternative deployment strategy. We selected Station North on Greenland (see also Figure 3) as the new deployment site, which is part of the ICOS atmospheric monitoring program. Colleagues from Aarhus University are in the process of upgrading the facilities to enhance its status within the European ICOS observation network. The MPG flask sampler, which has started its operation in September 2019 and has continuously provided data since, has been integrated into this concept. While deployment was originally intended to be temporary, travel restrictions due to the COVID-19 pandemic have prohibited site access during 2020/21, thus operation of the instrument remains at Station North for the time being.

### 2.1.2. Lessons learned and technology challenges identified during the project

Our experiment demonstrated that it is possible to operate the ICOS-manufactured automated flask sampler at remote Arctic sites without regular support from trained scientific staff. For our operations at Station North, trained scientists and technical staff from MPI-BGC and the ICOS-FCL only had access to the station for installation in September 2019. Due to COVID-19 related travel restrictions, for the about 21 months the instrument has been operational at the time of writing, the instrument could only occasionally be checked by scientific personnel from Aarhus University, who had no in-depth experience with the sampler itself. Standard operation was carried out by non-scientific military staff at Station North, without any major problems, instrument failures, or loss in data quality. We therefore conclude that this type of instrument is highly suited for long-term operation at remote Arctic sites, as long as regular instrument checks by reliable, non-technical personnel can be assured.



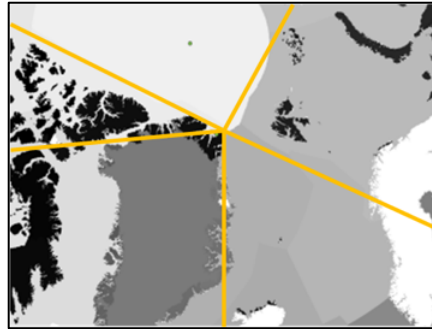


*Figure 4: Differentiation of five target domains, based on the prevailing wind direction. Starting from the lower left, the regions are labeled Greenland Ice Sheet, Canadian Arctic, Arctic Ocean, Barents Sea and Norwegian Sea.*

The benefits of equipping an atmospheric monitoring site with continuous observations of greenhouse gas mixing ratios with an additional automated flask sampler have been summarized in detail by Levin et al. (2020). In short, the flask data (i) can be used as a reference for quality-checking the continuous greenhouse gas observations, (ii) allow to monitor additional trace gas species not covered in the continuous program, and (iii) can be used also for monitoring  $^{14}\text{C-CO}_2$ , and therefore better constrain fossil fuel emissions contributing to the mixing ratio signals. While we did not analyze for  $^{14}\text{C-CO}_2$  at Station North, the main focus of our observations was placed on using additional trace gas signals like  $\text{O}_2/\text{N}_2$ , or isotopes, to better constrain the origin of sampled air masses. In this context, we tested a novel sampling strategy, reserving five flasks per sampling period to be slowly filled over a period of weeks with air from different source regions surrounding the sampling location (see also Figure 4). This long-term sampling, intended to provide integrated and representative trace gas fingerprints, successfully captured regional differences, and thus supports the interpretation of the origins of the data from instantaneous samples taken at scheduled intervals.

### **2.1.3. Description of processing and analysis of the obtained data**

At the time of writing, the automated flask sampler has been operational continuously for about 21 months, i.e. from September 2019 to June 2021. While samples were acquired during the entire period, so far only two deliveries of filled flasks have been returned to the institute for analysis, with a combined total of 90 filled flasks covering the period September 2019 to December 2020. For all samples received so far, the laboratory analyses at MPI-BGC in Jena have been finalized. The next shipment of filled flasks is currently being prepared, but most likely will not reach the institute before September 2021, i.e. too late to be included for INTAROS reporting.

#### ***Time series of trace gas mixing ratios***

Figure 5 summarizes the seasonal variability and mid-term trends for six major trace gases that are routinely quantified in the sampled flask air:  $\text{CH}_4$ ,  $\text{CO}_2$ ,  $\text{CO}$ ,  $\text{N}_2\text{O}$ ,  $\text{H}_2$ , and  $\text{SF}_6$ . The first four of these gases are part of the ICOS protocol for continuous measurements (operated by Aarhus University at Station North), so the flask sampler time series can be employed as an independent, high-precision data source to validate the performance of the gas analyzers. The two remaining gases, i.e.  $\text{H}_2$  and  $\text{SF}_6$ , provide novel data streams

that can provide valuable information for e.g. estimations of continental-scale flux rates based on atmospheric inverse modeling.

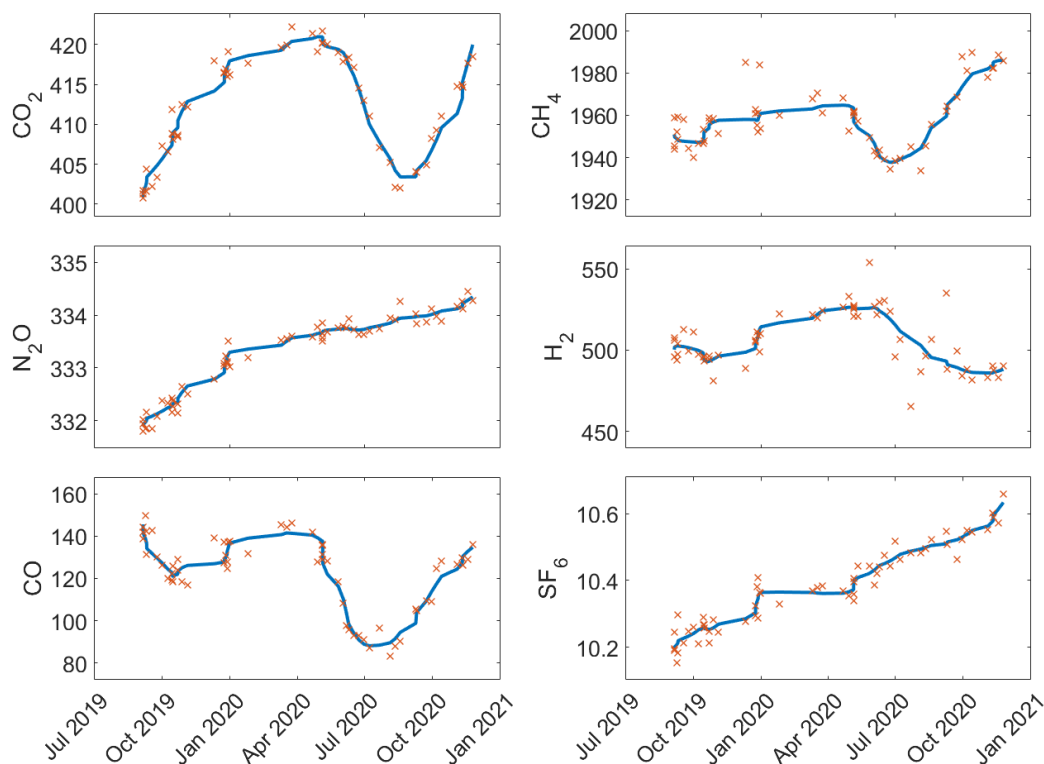
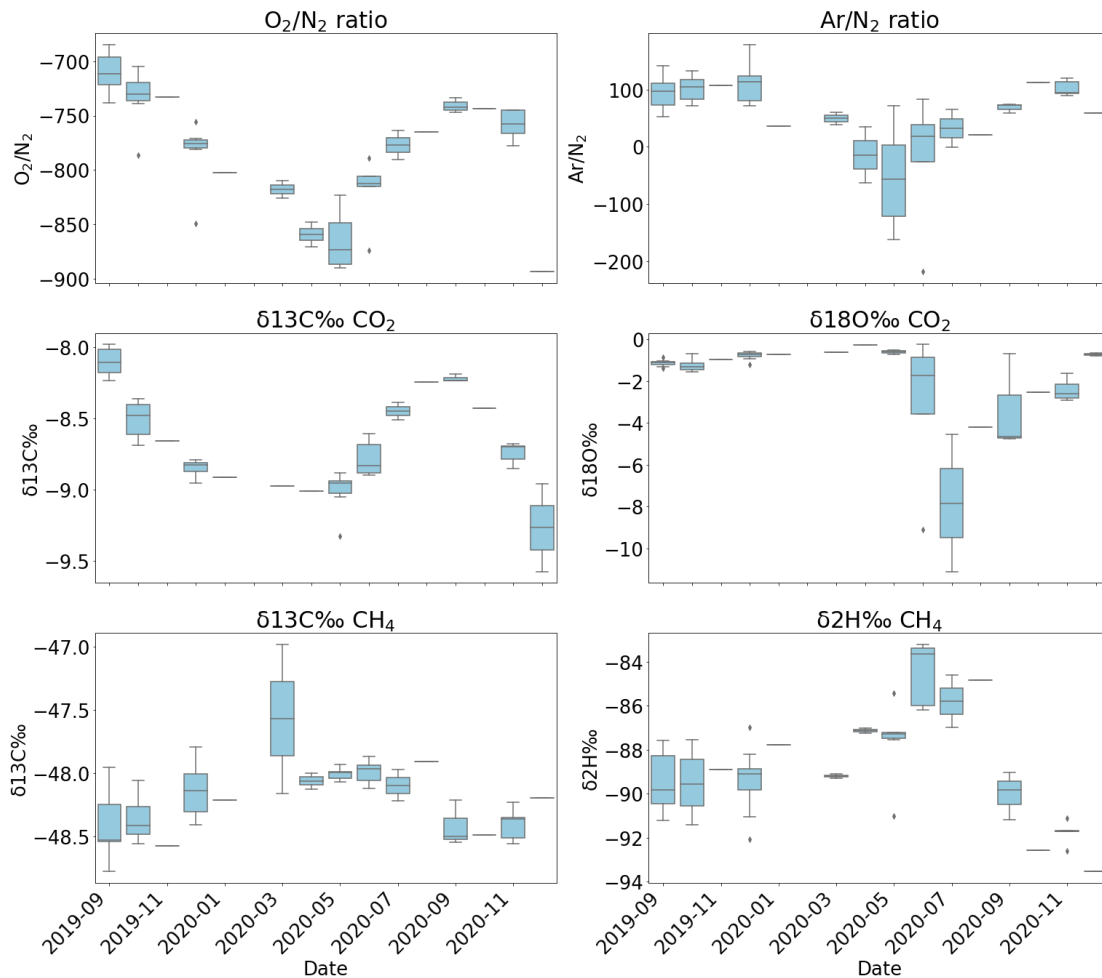


Figure 5: Integrated time series of GHG mixing ratios across all sampling strategies, with orange crosses indicating individual measurements, and blue lines a moving-window average to highlight seasonal variability and mid-term trends. Top row:  $\text{CO}_2$  and  $\text{CH}_4$ ; Center row:  $\text{N}_2\text{O}$  and  $\text{H}_2$ ; Bottom row:  $\text{CO}$  and  $\text{SF}_6$ .

The time series obtained so far for Station North, i.e. 16 months of data from September 2019 to December 2020, are not sufficient to reliably estimate trends, particularly for parameters like  $\text{CO}_2$  that exhibit a pronounced seasonal cycle. Still, for some parameters like  $\text{N}_2\text{O}$  or  $\text{SF}_6$ , relatively stable growth rates emerge from the data available so far, and particularly  $\text{SF}_6$  shows a marked increase in mixing ratio levels of about 4% over just 16 months within this remote Arctic location. To further interpret these signals, and determine sources that can be linked to the observed patterns in time series, atmospheric inverse modeling studies would need to be set up.

### ***Time series of trace gas ratios, and isotope signals***

Figure 6 summarizes the measured times series of the  $\text{O}_2/\text{N}_2$ ,  $\text{Ar}/\text{N}_2$  ratios, and the stable isotope signals for  $\text{CO}_2$  ( $\text{d}^{13}\text{C}-\text{CO}_2$ ,  $\text{d}^{18}\text{O}-\text{CO}_2$ ) and methane ( $\text{d}^{13}\text{C}-\text{CH}_4$ , and  $\text{d}^2\text{H}-\text{CH}_4$ ). These signals primarily aim to support the interpretation of large-scale representative concentration levels of these components, potentially improving estimations of their continental fluxes with the help of inverse modelling (e.g. Levin et al., 2020). These data become particularly interesting when comparing results between different source regions for the air masses sampled (see also Figure 7), and are discussed in more detail in the following sub-section.



*Figure 6: Time series of trace gas ratios (top row), CO<sub>2</sub> isotope data (center row) and CH<sub>4</sub> isotope data (bottom row). Boxes summarize observations at monthly timesteps, with horizontal bars showing the median, colored boxes the interquartile range, and whiskers the range between minimum and maximum observed trace gas levels, respectively.*

### ***Aggregated signals separating source regions of air masses***

The analysis of time-integrated signals from five different source regions demonstrates that our novel sampling strategy indeed is capable of capturing individual fingerprints in air mass composition, depending on the source region (Figure 7). Systematic differences were particularly identified for the isotopic signatures in the CH<sub>4</sub> molecules. CO<sub>2</sub> isotopes, on the other hand, revealed higher variability in the signals, with mostly overlapping ranges between regions.

The results displayed in Figure 7 are a promising indication that long-term integrated sampling of trace gas signatures can provide valuable insights into the specific source region signatures of air mass composition, and can therefore support the attribution of individual, instantaneously filled samples according to their origin, this way supporting the validation of atmospheric transport modeling.

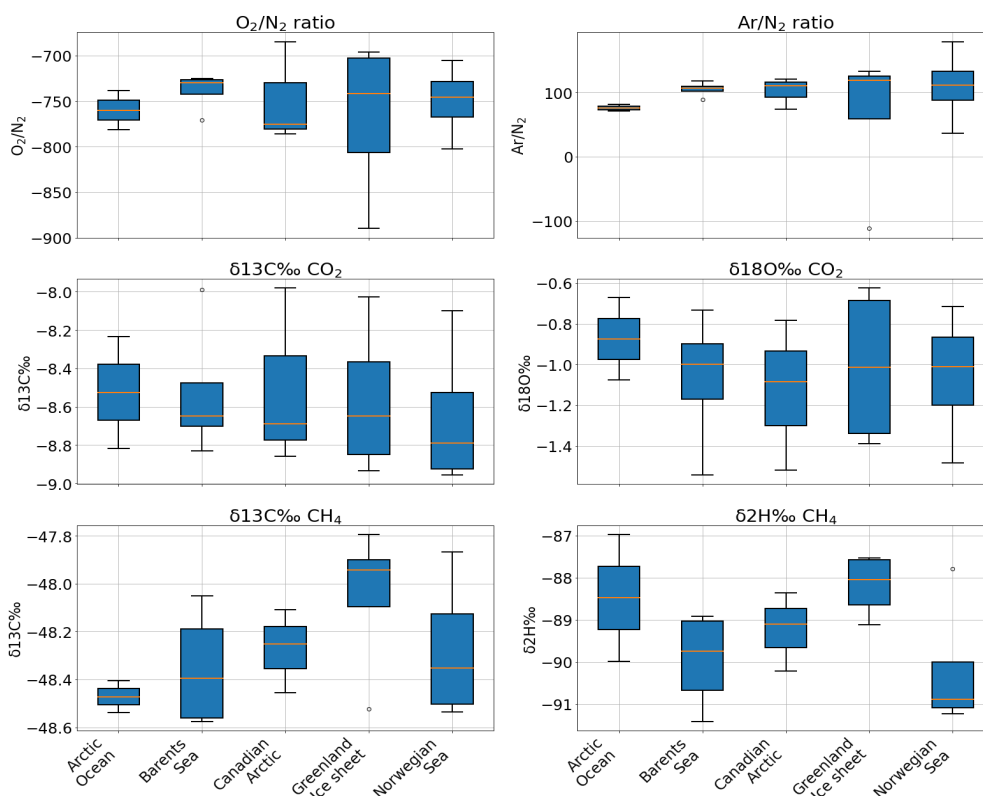


Figure 7: Signals of trace gas ratios (top row),  $CO_2$  isotope data (center row) and  $CH_4$  isotope data (bottom row) separated by source region of the air masses (see also Figure 4).

#### 2.1.4. Accessibility of the obtained data sets and repositories used

All datasets from the MPG flask monitoring program at Station North that have been finally analyzed at the time of writing were stored at the following repository:

DOI: <https://dx.doi.org/10.17617/3.6p>

The chosen host location, Edmond, is the Open Research Data Repository of the Max Planck Society. It serves the publication of research data from all disciplines, and enables secure provision, describing, documentation, linking, publishing and archiving of all kinds of data. The long-term availability of this repository is therefore assured.

We also aim at integrating our observations into the ICOS Data Portal (<https://www.icos-cp.eu/data-services/about-data-portal>). The assimilation of flask data into this repository, however, is still under development, therefore an upload is not possible at the time of writing.

#### 2.1.5. Future plans for operation of the observing system, including data provision

Plans for long-term operation of the automated flask sampler currently focus on a continued sampling campaign at Station North. The site provides excellent on-site personnel support, and manageable logistics based on the support of colleagues from ICOS and Aarhus University. Scientifically, the datasets obtained so far have demonstrated that Station North data provide highly interesting, high-quality signals from the High Arctic region, and help filling a gap in the Arctic monitoring program. However, funding for a continuation of the operation has not been secured at the time of

writing, therefore extension of the dataset will be dependent on future negotiations with ICOS and MPI-BGC, or successful acquisition of third-party funding. As long as the instrument is being kept operational, the data will be made available publicly through the same channels as outlined in Section 2.1.4 above.

## 2.2. GFZ

Contributors: Torsten Sachs, Katrin Kohnert, Andrei Serafimovich

### 2.2.1. Results of the final implementation of the observing system

The GFZ contribution to this task was to provide aircraft-derived vertical atmospheric profile data on temperature, humidity, CH<sub>4</sub> and partially CO<sub>2</sub> to assist in characterizing atmospheric transport and mixing processes. These observations are campaign-based by nature and in our case project-/proposal-based, and thus do not constitute an operational observing system in the sense of continuous or regularly scheduled observations. The contributed data are from past campaigns funded outside INTAROS.

We have conducted multiple airborne campaigns covering the Alaskan North Slope and the Mackenzie River Delta, Canada. Scalar mixing ratios and temperature profiles have been processed consistently for the 2012 – 2013 campaigns.

The campaigns were based out of Utqiagvik (formerly Barrow) for growing season coverage of the Alaskan North Slope and out of Inuvik for coverage of the Mackenzie River Delta and adjacent coastal plains. They primarily aimed at regional estimates of greenhouse gas fluxes (see INTAROS reports D2.7 and D2.8) by airborne eddy covariance based on horizontal flight tracks in about 40 m – 80 m above ground level. Vertical profile flights within and above the atmospheric boundary layer were done at the beginning and end of each flight track to detect the thickness of the boundary layer, ranging from several hundred meters to >2000 m altitude.

We used the research aircraft Polar 5 owned by the Alfred Wegener Institute – Helmholtz Centre for Polar and Marine Research (AWI). Greenhouse gas concentrations were measured in sample air drawn from an inlet tube at the top of the cabin at about 9.7 l s<sup>-1</sup> and analyzed at 20 Hz in an RMT-200 (Los Gatos Research Inc., Mountain View, California, USA) in 2012 (CH<sub>4</sub> concentration only) and in a Fast Greenhouse Gas Analyzer FGGA 24EP (Los Gatos Research Inc.) from 2013 onwards (CH<sub>4</sub>, CO<sub>2</sub> and H<sub>2</sub>O). Air temperature was measured with an open wire Pt100 in an unheated Rosemount housing. A full description of the system set-up can be found in Hartmann et al. (2018).

Almost 300 individual vertical profiles were extracted from the continuous data sets of 2012 and 2013 and stored in 1 Hz temporal resolution with a UTC time stamp. Position data are provided in decimal degrees, the altitude is given as GPS altitude and needs to be converted to altitude above ground level if of interest for the user. In addition to atmospheric pressure (in hPa), air temperature (in °C) and the 3D wind vector (in m s<sup>-1</sup>) are provided as well as CH<sub>4</sub> concentrations in wet mole fractions and H<sub>2</sub>O concentrations in dry mass fractions.

### **2.2.2. Lessons learned and technology challenges identified during the project**

This system has been operational since before INTAROS, thus there are no specific challenges identified during the project. However, it should be noted that a sensor warm-up phase of up to 45 minutes was needed for the gas analyzer. Occasionally sensors could be pre-heated by ground power, but this was not always available.

Originally, it was envisioned to also provide profile measurements from the Lena River Delta region, Siberia, taken in 2012 and 2014 using a helicopter-towed airborne eddy covariance system. The quality control and raw data re-processing undertaken during INTAROS, however, revealed serious issues with the altitude and position raw data. It is currently unclear whether the data are salvageable at all. That assessment and any possible subsequent correction and re-processing of the data require a lot more resources and is not an option anymore within this project.

In addition to this unforeseen issue, the primary challenge during the project were early departures by project scientists and delays caused by difficulties in finding adequate replacements as well as the pandemic interruption of normal business.

### **2.2.3. Description of processing and analysis of the obtained data**

The general processing of the data (including flux data and profile data) is described in detail in Hartmann et al. (2018), covering position and velocity, temperature and humidity, the gas analyzers, data acquisition, and all calibration and alignment procedures. A repetition would exceed the scope of this report.

### **2.2.4. Accessibility of the obtained data sets and repositories used**

All data will be openly available in Pangaea under their campaign acronym and year (AIRMETH\_YYYY). Each individual data set will be given a unique DOI and can be directly downloaded.

### **2.2.5. Future plans for operation of the observing system, including data provision**

There are currently no robust future plans for additional campaigns, primarily due to lack of financial and staff stability.

## **2.3. UNEXE**

Contributors: Walter Oechel, Alyssa Mease, Marco Montemayor

### **2.3.1. Results of the final implementation of the observing system**

We installed a new heated sonic anemometer (CSI\_CSAT3BH) in Barrow, Alaska, during summer 2019. The goal was to collect continuous CO<sub>2</sub> and CH<sub>4</sub> fluxes during the entire year, with a particular focus on the fall and winter, which are the most uncertain times of the year in terms of both CO<sub>2</sub> and CH<sub>4</sub> emissions.

### 2.3.2. Lessons learned and technology challenges identified during the project

In our study, we found fall CH<sub>4</sub> emissions to be higher during the zero-curtain period than after soil freezing across all sites and years measured. This is consistent with the temperature dependence of CH<sub>4</sub> production that has been well documented in incubation experiments. The temperature sensitivity of CH<sub>4</sub> production has been found to be different below freezing than above freezing which could aid in explaining why there is a sudden drop in CH<sub>4</sub> emissions after soil freezing. We observed the warmest site (Ivotuk, US-Ivo) to have the highest flux rates both before and after freezing. However, Atqasuk (US-Atq), which is the next warmest, has the lowest flux rates, likely due to low soil moisture (~40% VWC) and sandy soils providing poor habitat for CH<sub>4</sub> production despite higher temperatures. Sandy soils can further allow higher gas diffusion rates, which, given low moisture content like those at the US-Atq site, support the diffusion of oxygen where methanotrophs can thrive and consume a large portion of the CH<sub>4</sub> produced.

One of the most important results of our research was the collection of substantial methane emissions after freezing, likely due to the presence of liquid films in pore spaces and cold adapted microbial communities. We showed that CH<sub>4</sub> emission during the zero-curtain period can account for over 20% of the annual CH<sub>4</sub> budget in Arctic ecosystems, with the total cold season accounting for around 50%. Figure 8 highlights the importance of the emissions during the zero curtain comparing to the summer (Hashemi et al., 2021).

Unfortunately, we realized that the heating of the CSI\_CSAT3BH was not appropriate to completely de-ice the sonic anemometer during the fall and winter, which resulted in large data losses, particularly during spring 2020 when we were not able to access the sites. Therefore, we ordered two new call A METEK sonic anemometers. These new instruments have an implemented de-icing, which is activated based on both air temperature signals and data quality. We are currently in the process of programming the data acquisition of these new sonic anemometers, and we are planning to install them in the field in summer 2021 in two sites of this research program.

### 2.3.3. Description of processing and analysis of the obtained data

The measured variables include CO<sub>2</sub> and CH<sub>4</sub> fluxes together with air temperature, and the three wind components collected at 10 Hz used to estimate the eddy covariance fluxes. Additionally, a variety of environmental variables (soil moisture, soil heat flux, net radiation, etc.) were also collected and averaged to 30 minutes and then daily timesteps to provide an estimate of the temporal trends of the main variables that control the CO<sub>2</sub> and CH<sub>4</sub> fluxes. A post-processing was performed using the following criteria: the initial quality check was done following Mauder and Foken (2015), where low quality data indicated with a quality flag of “2” were removed. For sites with LGR FGGA gas analyzers, fluxes where internal instrument chamber pressure was greater than or equal to 155 torr were removed as it indicated instrument failure. A turbulence threshold ( $u^*$ ) was also applied where data with  $u^*$  less than 0.1 ms<sup>-1</sup> were removed (Reichstein et al., 2005). A moving window of two weeks was applied and fluxes that were three standard deviations away from the mean were removed as outliers.

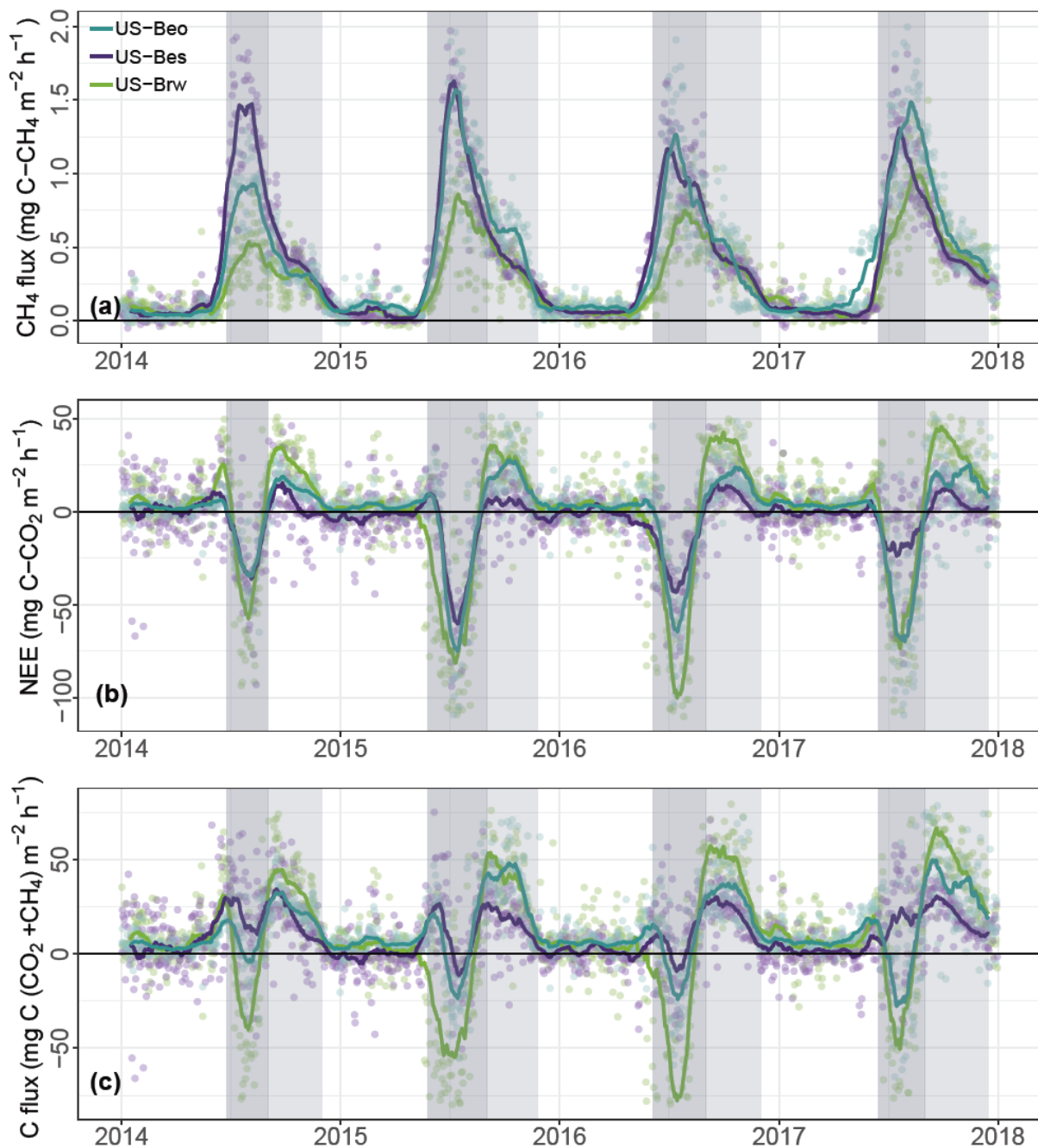


Figure 8: Carbon flux (daily average) of (a) CH<sub>4</sub>, (b) CO<sub>2</sub>, and (c) CO<sub>2</sub> + CH<sub>4</sub> (with CH<sub>4</sub> expressed as CO<sub>2</sub>-eq based on warming potential) at the three EC sites. The darker shaded portion represents the growing season, while the lighter shaded portion represents the zero-curtain period.

### 2.3.4. Accessibility of the obtained data sets and repositories used

The CO<sub>2</sub> and CH<sub>4</sub> fluxes, and environmental variables collected during the duration of the project are stored in the Arctic Data Center:

<https://arcticdata.io/catalog/view/doi%3A10.18739%2FA2X34MS1B>

This is a data repository which is freely accessible and receives long term funding from the National Science Foundation (NSF), so it will continue to provide access to the data after the end of the INTAROS project.



### **2.3.5. Future plans for operation of the observing system, including data provision**

The measurements detailed here will continue to be collected after the end of the INTAROS project for another 5 years funded by the AON NSF grant:

[https://www.nsf.gov/awardsearch/showAward?AWD\\_ID=1932900](https://www.nsf.gov/awardsearch/showAward?AWD_ID=1932900)

The data collected during these additional 5 years will be submitted to the Arctic Data Center as listed above (at the same link which will automatically update the dataset).

## **2.4. USFD**

Contributors: Donatella Zona

### **2.4.1. Results of the final implementation of the observing system**

In summer 2016, we installed two high spatial and temporal resolution temperature profiles at the Alaskan sites Atqasuk (US-Atq) and Ivoituk (US-Ivo) to better characterize the soil freezing and the persistence of unfrozen soils during the cold period. A third system was installed at the US-Bes site near Utqiagvik during summer 2018. These profiles included thermocouples every 5 cm from 25 cm above the surface to 90 cm below the surface at US-Ivo and US-Atq and 75 cm below the surface at US-Bes. Data were recorded on a CR6 data logger (Campbell Scientific®) with four AM25T multiplexers (Campbell Scientific®) at US-Ivo and US-Atq and a CR1000 data logger (Campbell Scientific®) with three AM25T (Campbell Scientific®) multiplexers were used at the US-Bes site. The thermocouples measured temperatures at two Hertz; the half hour average of these measurements was recorded.

### **2.4.2. Lessons learned and technology challenges identified during the project**

Our results show that the presence of unfrozen soil layers is lasting longer into the cold season over the last decades, and that the duration of the zero curtain can sometimes persist well into January, after the soil surface is frozen and the air temperature is well below zero. Soil moisture content proved to be a dominant control on soil freezing, considering that the development and persistence of the zero-curtain conditions are linked to latent energy released during freezing. Wetter conditions were linked to deeper thaw due to higher conductive heat transfer, which may further delay complete freezing given a larger active layer.

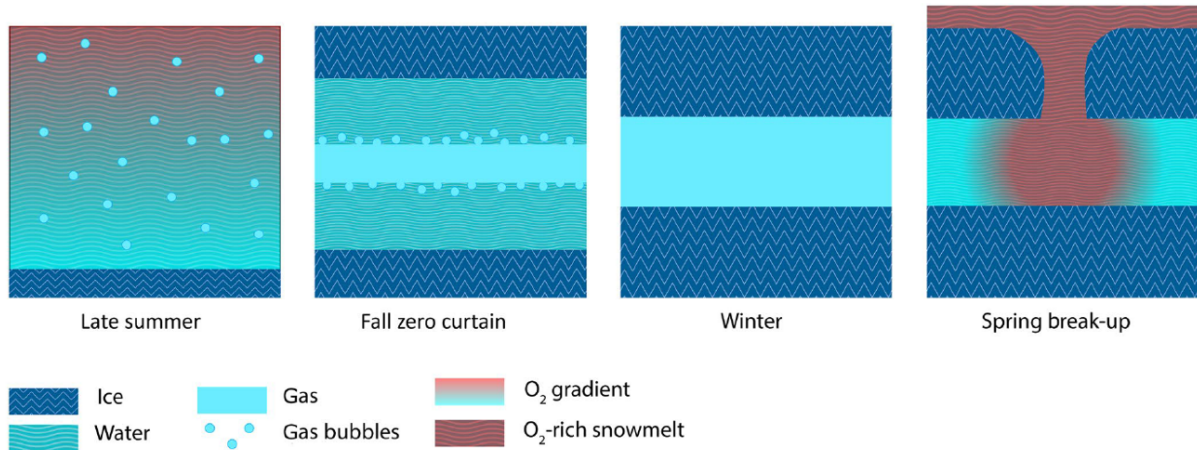


Figure 9: Seasonal phase changes in the soil profile leading to oxygenation and convective heating in spring. In late summer, the soil profile is saturated, growing anoxic with depth. Small circles represent dissolved gases. During the zero-curtain period in the fall, water migrates to the upper and lower freezing fronts and gases are driven out of solution, leading to unsaturated voids in the middle of the profile in winter. In spring, snow melt can penetrate these pockets, bringing oxygen to lower layers and causing rapid warming (Arndt et al., 2020).

Our data supports these studies in that the wetter sites generally froze on a later date than the dryer sites and that soil moisture was a significant factor in predicting when freezing may occur across the sites. The high-resolution soil temperature profiles collected with the support of this project showed how long deeper soil temperatures may remain unfrozen (near 0°C) while air temperatures drop to -20 °C to -30 °C. Shallower soil temperatures largely underestimated the persistence of deeper unfrozen soils up to 96 days (see figures below, Arndt et al., 2019).

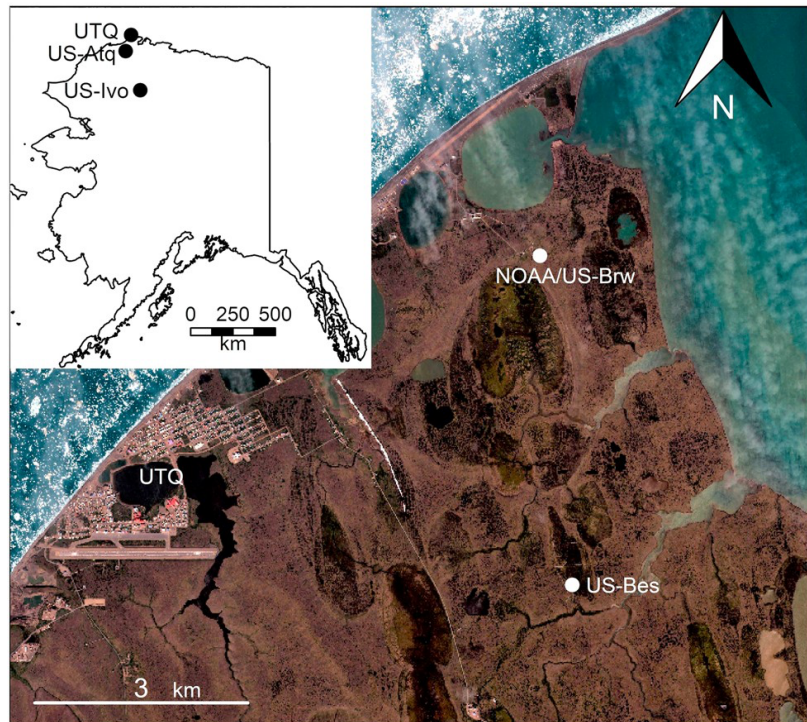


Figure 10: WorldView-2 (Digitalglobe™) true color image of the Utqiagvik (UTQ) region and an AK map inset showing the location of the eddy covariance tower sites and National Oceanic and Atmospheric Administration (NOAA) BRW station in Alaska (Arndt et al., 2019).

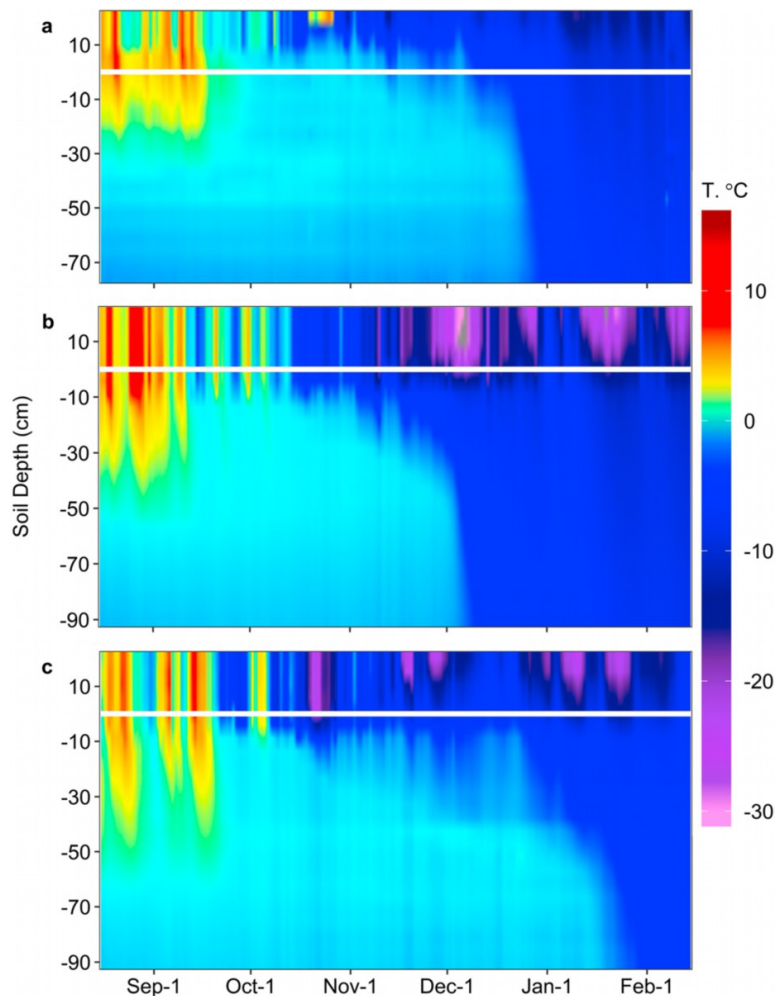


Figure 11: Soil temperatures measured with thermocouples every 5 cm at US-Bes, US-Atq, and US-Ivo (a, b, and c, respectively) to show ZCF relationships at depth. The ZCF, represented by cyan, shows freezing fronts from the top and bottom of the soil profile.

The main challenge we faced in 2020 was that we were not able to access the sites and solve problems to the data collection of several sensors that needed servicing, which resulted in large gaps in the data available for the fall and winter 2019 and the entire 2020.

#### 2.4.3. Description of processing and analysis of the obtained data

We measured soil temperature at a fine resolution to characterize the soil freezing during the fall, and the persistence of unfrozen soil layers later in the fall. The data were averaged over 30 minutes. We applied a data cleaning based on the standard deviation (and data outside of a 3 standard deviations threshold were removed).

#### 2.4.4. Accessibility of the obtained data sets and repositories used

The high-resolution soil temperature data collected during the duration of the project are stored in the Arctic Data Center:

<https://arcticdata.io/catalog/view/doi%3A10.18739%2FA25X25C75>

This is a data repository which is freely accessible and receives long term funding from the National Science Foundation (NSF), so it will continue to provide access to the data after the end of the INTAROS project.

#### **2.4.5. Future plans for operation of the observing system, including data provision**

We are planning to access the field in summer 2021 with the goal to reestablish data collection and data transfer. Once data transfer will be reestablished, we are planning to add the additional 2019 -- 2021 data to the Arctic Data Center as listed above.

The measurements detailed here will continue to be collected after the end of the INTAROS project for another five years funded by the AON NSF grant:

[https://www.nsf.gov/awardsearch/showAward?AWD\\_ID=1932900](https://www.nsf.gov/awardsearch/showAward?AWD_ID=1932900)

Data collected for these additional five years will be submitted to the Arctic Data Center and the same link included above (which will automatically update the dataset to include more recent data).

## **2.5. CNRS-Takuvik**

Contributors: Florent Domine, Denis Sarrazin, Georg Lackner

### **2.5.1. Results of the final implementation of the observing system**

Our objectives were focused on (1) obtaining fairly holistic time series of physical environmental variables allowing the investigation and detection of novel climatic feedbacks and the testing of land surface models and in particular their snow schemes; and (2) contributing to a data base of soil and permafrost carbon stocks and understanding the impact of shrub expansion (a.k.a. Arctic greening) on soil carbon stocks. During this project we therefore deployed or improved monitoring instrumentation for soil, snow and atmosphere at four sites in the Canadian High Arctic at 55, 56, 73 and 83°N (Figure 12).

For the 55 and 56°N sites, we have a continuous data record. For the 73°N site, the data stop in June 2019 because we could not access the site in 2020 and access in 2021 is uncertain. For the 83°N site, it could not be accessed since 2019 either and we also had some instrument failure due to the extreme conditions in the very remote and inaccessible site. Remarkable monitoring data include time series of snow and soil thermal conductivity (Figure 13) as well as reasonably reliable radiation data.

Obtaining radiation data in the Arctic is difficult because winter frosting compromises data and providing heating is a problem for remote instruments in the polar night. Our compromise was to heat and ventilate the radiometer for five minutes every hour and take a measurement then.



and biomass by  $4 \text{ kg m}^{-2}$ .

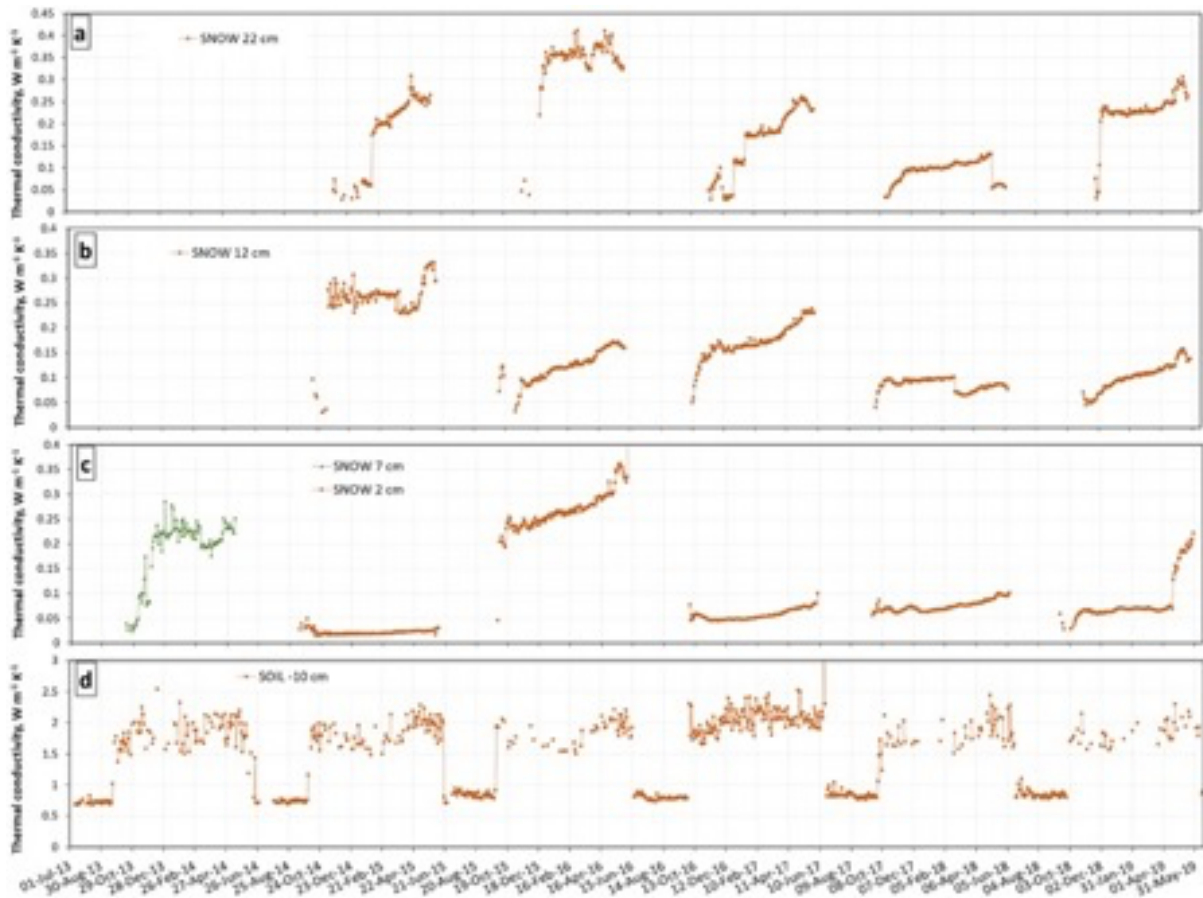


Figure 13: Time series of snow thermal conductivity at three heights at the Bylot herb Tundra site (73°N) and of soil thermal conductivity at 10 cm depth. For snow, year to year variability is observed. Besides application to the permafrost thermal regime, these data are being used for ecological application. For example, the thermal conductivity of the basal snow layer (c) is a proxy for its hardness. Since lemmings, a key species in Arctic terrestrial ecology, live at the base of the snowpack, years with a hard basal snow layer have been found to coincide with population crashes because lemmings have difficulty accessing food and reproducing in hard snow. Snow studies are therefore useful to understand lemming population dynamics.

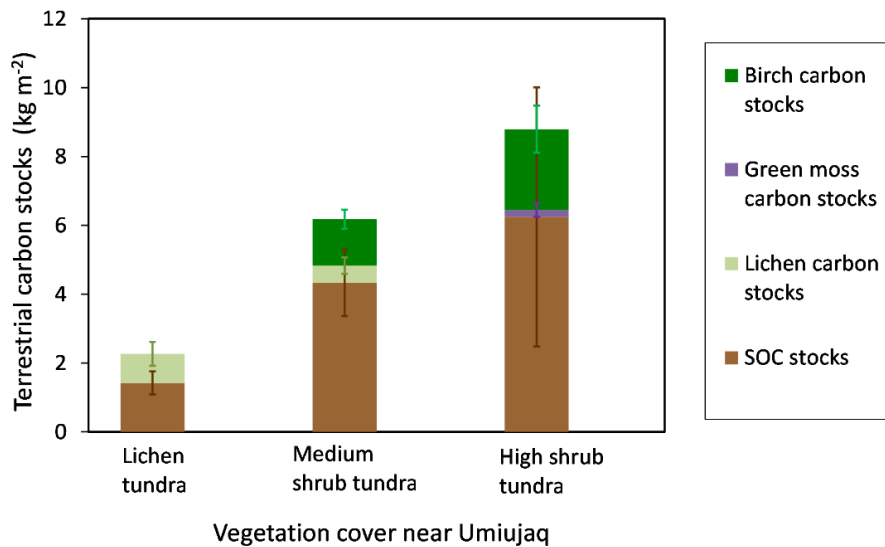


Figure 14: Soil C stocks near Umiujaq, 56°N, as a function of vegetation cover. The growth of medium shrubs (60 cm high) on lichen tundra results in an increase in C stocks of 4 kg m<sup>-2</sup>. Further shrub growth (100 cm) lead to the substitution of the lichen understory by moss and to a further C stock increase of 2 kg m<sup>-2</sup>.

### 2.5.2. Lessons learned and technology challenges identified during the project

The main lesson learned is to avoid relying totally on data loggers and instruments from Campbell Scientific. Their products are for the most part good and reliable, but they are complicated and can only be maintained by highly skilled personnel. In the pandemic situation, this has proven catastrophic, as no one is trained for this amongst locals in the Canadian North. Furthermore, we have discovered serious issues with some Campbell instruments, which the manufacturer had not reported, such as a bug in the program supplied to run the CNR4 radiometer. We will therefore deploy less expensive and simpler backup instruments, such as from METER. It would also be highly desirable to have remote access to the data, but the mass of data produced makes this very expensive. Satellite remote access is also a serious problem at 83°N.

Lastly, frosting of the upper sensors of the CNR4 in winter has been found to be a problem, as the five minutes of hourly heating provided is often insufficient during the polar night. Of course, for shortwave radiation this is not important, as there is nothing to measure. However, longwave downwelling radiation has been found to be unreliable. Figure 15 shows raw data (i.e. before correction for the sensor temperature) from the upper pyrgeometer of the CNR4. This indicates ice condensation by frosting on the pyrgeometer glass. Much longer heating times would be required but this is really an issue regarding power supplies. Solar panels of course do not work. We do have a wind mill, but the site is not very windy. We are exploring options to attempt to improve the situation.

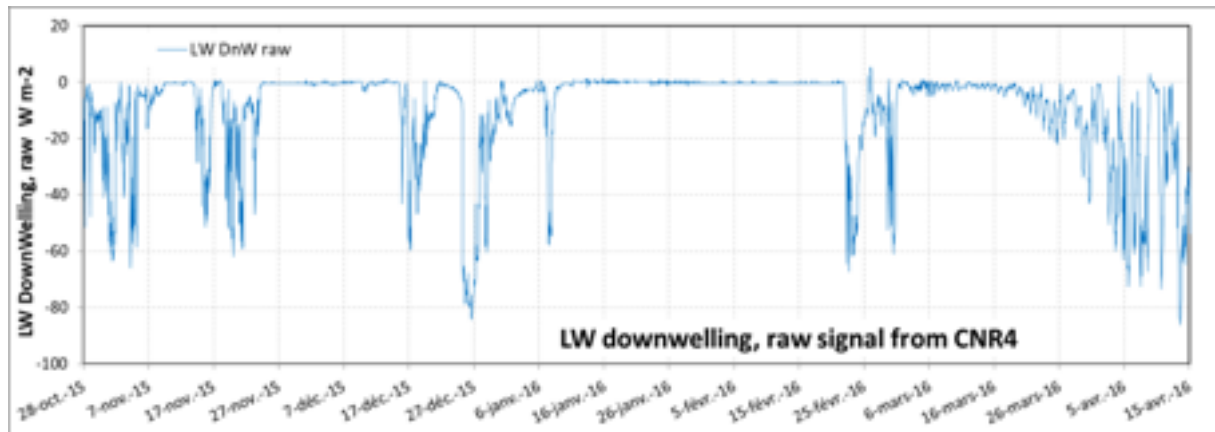


Figure 15: Raw data from the upper pyrgeometer of the CNR4 during the 2015-2016 winter. For most of the winter, data indicate 0 LW flux. We interpret this as ice frosting forming in the top of the pyrgeometer. The LW flux measured is that of the ice on the glass rather than that of the atmosphere above. Since the ice is essentially at the same temperature as the CNR4, the flux is 0. A hybrid data set with corrected reanalysis data from ERA5 has been constructed to resolve this problem.

### 2.5.3. Description of processing and analysis of the obtained data

Atmospheric variables measured were air temperature and relative humidity, wind speed and direction, upwelling and downwelling shortwave and longwave radiation. Snow variables monitored were snow height and snow temperature and thermal conductivity at several heights. Soil variables measured were thermal conductivity, temperature and liquid water content at several depths. Data were carefully checked and quality-controlled as detailed in Domine et al. (2021). For example, relative humidity data were corrected to ensure that maximum values reached the ice saturating vapor pressure. Radiation data were compared to ERA5 reanalyses and data gaps in downwelling long wave radiation were filled using ERA5 values modified following a correlation between our values and ERA5 values. Incidentally, ERA5 values were found to be  $25 \text{ W m}^{-2}$  too low at our spot. Thermal conductivity data were analyzed as detailed in Domine et al. (2015).

### 2.5.4. Accessibility of the obtained data sets and repositories used

Data files for at least three of our four sites will be prepared. For the moment we have produced data files for forcing and validating land surface models and snow models for our High Arctic site of Bylot Island ( $73^{\circ}\text{N } 80^{\circ}\text{W}$ ).

The data file from Bylot Island for driving and validating land surface and snow physics model is available on the Nordicana D repository at: <https://doi.org/10.5885/45693CE-02685A5200DD4C38>.

We have also analyzed soil and permafrost samples from Bylot Island, in order to produce carbon and nitrogen stock data, which will also be placed on the Nordicana D repository.

### 2.5.5. Future plans for operation of the observing system, including data provision

Time series initiated before and during this project will be continued inasmuch as possible; however, we are worried about the data gaps caused by the pandemic, since a significant interest of time series is their completeness. Regarding ECVs, we will provide time series of air temperature, relative humidity, wind speed and downwelling radiation



for four sites. At two of these sites, we actually have meteorological stations at several locations in different vegetation types. At Bylot Island we have data for a herb tundra site and for a shrub tundra site. At Umiujaq we have data for a lichen tundra site and for a forest tundra site. We will also provide soil temperature data at a total of twelve locations for our four sites, from polar desert to northern boreal forest.

## 2.6. FMI

Contributors: Roberta Pirazzini, Juha Lemmetyinen, Teijo Arponen, Henna-Reetta Hannula, Anna Kontu, Jorge Ruiz, Riku Tarvainen

### 2.6.1. Results of the final implementation of the observing system

The FMI Sodankylä-Pallas research station (67.367°N, 26.629°E) is a cal/val site for the NASA SMAP and ESA SMOS missions, representing the boreal forest zone. It hosts a unique infrastructure for long-term multidisciplinary measurements: soil, ecosystem, cryosphere, and atmosphere (troposphere, clouds stratosphere, ionosphere). The site is part of integrated atmospheric networks such as GAW, ACTRIS, IASOA and EMEP. To achieve a better exploitation of satellite observations and fulfil the modelling needs for the development of new, multi-sensor retrieval methods, the observation system was integrated with new instruments. The contribution of INTAROS to this enhancement of the observational capacities consisted of the testing of new devices (purchased with other funding) and the development of the data acquisition and processing chain (measurement protocol, data quality control, software for raw data processing, data format and storage).

#### *The SodScat scatterometer*

The SodScat scatterometer is built around a Vector Network Analyzer (VNA). The scatterometer unit of the system is protected by an outer case, which beside the VNA includes also internal temperature control, temperature and humidity monitoring, humidity control, and an RF unit. In addition, the system includes control computer, external RF cable harness, horn antennas, and a Power Supply Unit (PSU). The system is fully polarimetric and operates in the 1 – 10 GHz frequency range (L- to X-band), which covers the frequency range used by most operational SAR systems (e.g. ALOS2, Sentinel-1, TerraSAR-X/TanDEM-X).

The SodScat radar was installed on a new 24-m observation tower at the FMI-ARC in the summer of 2018 (Figure 16). The tower, built as a part of the Integrated Carbon Observing System (ICOS), hosts a variety of sensors for monitoring CO<sub>2</sub> and CH<sub>4</sub> flux and concertation, radiation and thermal balance, as well as snow, soil and atmospheric properties. This enables cross-cutting studies with observing changes in CO<sub>2</sub> emission by means of proxy parameters derived from microwave remote sensing (e.g. snow cover and soil properties and their relation to the carbon balance).



Figure 16: Microwave instrumentation installed on the top platform of the ICOS tower at FMI-ARC. SodScat is lowermost, attached on a rail at the base of the platform.

The SodScat installation enables continuous measurements (several daily observations) of the active microwave response of the boreal forest landscape in controlled conditions. The tower (Figure 16) overlooks a boreal forest site dominated by Scots Pine (*pinus sylvestris*) of varying age (60 – 160 years). Installed at the height of 21 m, SodScat provides observations from above the forest canopy, enabling remote sensing studies related to retrieval of surface parameters over forested areas (where the forest canopy poses a challenge) as well as for retrieval of vegetation parameters themselves (forest biomass and height, vegetation optical depth and water content). The tower hosts also passive microwave instruments (radiometers) at 1.4, 10.65, 18.7, 21 and 37 GHz, enabling combined active-passive measurements of the same scene. Installed on a 5 m rail, SodScat can operate also as a SAR providing an image of the observed scene at the desired frequency bands. SAR imaging is the current default data acquisition mode; a SAR image at four frequency bands (L, S, C and X) and two polarizations (VV, VH) is acquired every 12 hours.

Table 1 summarizes the microwave instrumentation installed on the ICOS tower. All instruments provide frequencies relevant for several existing satellite systems. Note that while the SodRad and SodScat systems are owned by FMI, the Elbara-II radiometers and the WBScat radar are currently on loan from the European Space Agency (ESA).

Table 1: Microwave instrumentation installed at FMI-ARC ICOS tower.

Instrument name	Type	Frequencies	Owner	Reference Satellite system	Notes
SodScat	Microwave radar	1-10 GHz	FMI	Sentinel-1, RCM, Cosmo-SKYMED, TerraSAR-X /Tandem-X.	Azimuth and elevation scan capability (scatterometer mode)  SAR imaging capability by displacement rail (5 m aperture)

SodRad	Microwave radiometer	10.65, 18.7, 21.0, 36.5 GHz	FMI	SSMIS, AMSR2,	Dual polarization, azimuth and elevation scan capability
Elbara-II	Microwave radiometer	1.4 GHz	ESA	SMOS, SMAP	Two systems installed (above and below canopy). Dual polarization, elevation and azimuth scan capability
WBScat	Microwave radar	1-40 GHz	ESA	Sentinel-1, RCM, Cosmo-SKYMED, TerraSAR-X /Tandem-X + future missions	On loan from ESA, operated by WSL

### ***The SVC-FMI spectro-albedometer***

The SVC-FMI spectro-albedometer was installed over a flat, snow-covered wetland site and measured incoming and reflected spectral irradiance and their ratio, the albedo, at high spectral and temporal resolution for about one month during three consecutive springs (2019 – 2021, Figure 17). The installation setup was constructed in advance, before the snow accumulation, so that the observed field remained undisturbed during the positioning of the instrument. To fully test the instrument and exploit the measured spectra, other continuously measuring broadband and spectroradiometers were installed in the same field and intensive measurements of snow macro- and micro-physical snow properties were carried out once or twice a day. In addition to the field measurements, laboratory measurements were carried out to calibrate and characterize the instrument. Procedures to correct for the thermal drift of the sensor sensitivity (thermal correction), the deviation from the perfect cosine response (angular correction) and for shadows/obstructions of the field of view caused by the supporting structure were developed, enabling the assessment and minimization of the measurement uncertainty. These procedures will be integrated in the automatic data processing that will convert the raw data into calibrated and corrected spectra of irradiances and albedo in near-real time.



Figure 17: SVC-FMI spectro-albedometer installed in Sodankylä, Finnish Lapland.

## 2.6.2. Lessons learned and technology challenges identified during the project

### *The SodScat scatterometer*

Running a ground-based radar system in Arctic conditions has proven to be challenging, but feasible. While instrument electronics can be shielded from environmental conditions with relative ease, moving parts necessitated by the radar system and SAR imaging such as the displacement rail and 3-axis positioner of SodScat are prone to mechanical failures in cold conditions as well as water condensation and ice buildup during spring melt-refreeze cycles. Particular attention should be placed in construction of additional mechanical shielding, heating systems and the application of Arctic-quality lubricants to any moving mechanical parts.

### *The SVC-FMI spectro-albedometer*

The developed measuring system, with the weather-proof enclosure, internal heating, and ventilation of the domes to prevent frost formation has proven to withstand harsh winter conditions in the terrestrial Arctic and can be applied for continuous measurements with minimal maintenance effort. The single spectro-radiometer connected to two integrating spheres to sequentially collect the incoming and reflected irradiance demonstrated to be a robust solution, economically convenient compared to having two spectroradiometers to separately measure the incoming and reflected irradiance. So far, similar instruments that automatically provide irradiance and albedo for the whole solar spectrum (350 – 2500nm) at high spectral resolution (2 – 10nm) are not commercially available. The commercially available automatic spectroradiometers that can be used in the Arctic cover only the visible and near-infrared wavelength region (350 – 950 nm), leaving out the wavelengths for which snow albedo is lowest (1000 – 2500) and which contributes to more than half of the net shortwave radiation absorbed by the snow (Pirazzini et al., 2015). The albedo in these longest wavelengths of the solar spectrum is very sensitive to changes in surface roughness and optical equivalent grain size (which evolve with the snow metamorphism), and therefore being able to monitor it is very important for the quantification of the surface radiation and energy budget. The

developed instrument has therefore the potential of covering an existing measurement gap.

### 2.6.3. Description of processing and analysis of the obtained data

#### *SodScat scatterometer*

The basic measurement protocol of SnowScat Microwave backscatter (and phase) at bands of 1 – 2 GHz, 3 – 4 GHz, 5 – 6 GHz, and 9 – 10 GHz at two polarization configurations (VV, VH). Measurements are performed every 6 hours, alternating between like- and cross-polarization (VV and VH). Each scan spans four hours. An example acquisition is depicted in Figure 18.

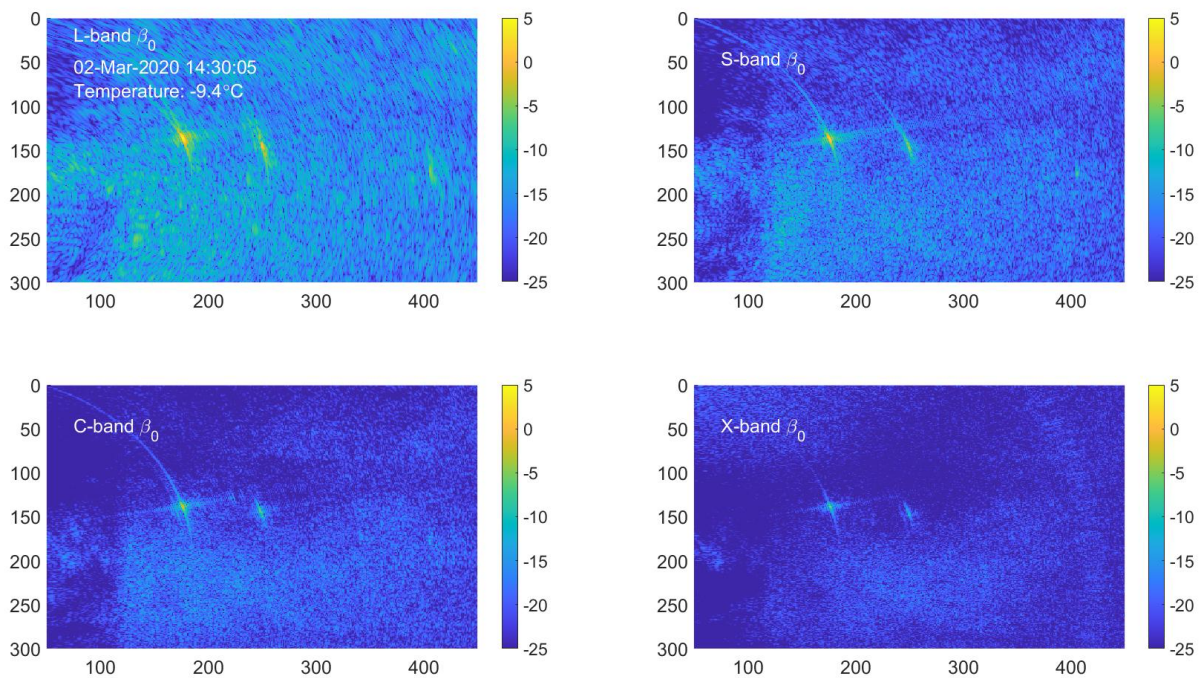


*Figure 18: Example of SAR data at L-X bands acquired using the SodScat system. Two corner reflectors used for calibration are visible in the images as “bright” areas.*

SodScat data are radiometrically calibrated using external calibration targets (trihedral and dihedral corner reflectors). A trihedral reflector with an edge length of 90 cm for co-polarization and one tilted dihedral reflector with squared faces of 30 cm for cross-polarization are applied. The targets are located in clear line of sight from the radar on its full aperture. The external targets are also used to monitor stability of the system during operation. Receiver stability is also monitored using a separate internal calibration loop.

A SAR image can be reconstructed from SodScat observations taken in sequence along the displacement rail perpendicular to range direction. After collection of samples along the rail, the measurements can be treated as if they were performed by a phased array; they are coherently summed with appropriate phase shifts to form the narrow receive beams in each spatial location of the scene (image pixel). This procedure can be repeated for each spatial location of interest.

To obtain a high spatial resolution in range (radial distance from the radar), the radar needs to transmit a pulse of a short time duration. Alternatively, a large bandwidth corresponding to a short pulsewidth can be synthesized by transmitting a frequency modulated signal. SodScat is operated in a SFCW mode to obtain a large frequency bandwidth for the signal. During a frequency sweep, the system sequentially transmits a discrete set of equally spaced frequencies. For each CW frequency segment, the signal is down-converted and averaged to obtain a single IQ sample.

### ***SVC-FMI spectro-albedometer***

The instrument measures incoming irradiance, reflected irradiance, and surface albedo spectra in the 350 – 2500 nm wavelength range at 3 – 10 nm resolution every two minutes. The raw data collected every two minutes include:

- Counts of photons detected by the instrument after receiving the signal from the upward looking integrated sphere - Spectrum of incoming irradiance.
- Counts of photons detected by the instrument after receiving the signal from the downward looking integrated sphere - Spectrum of reflected irradiance.

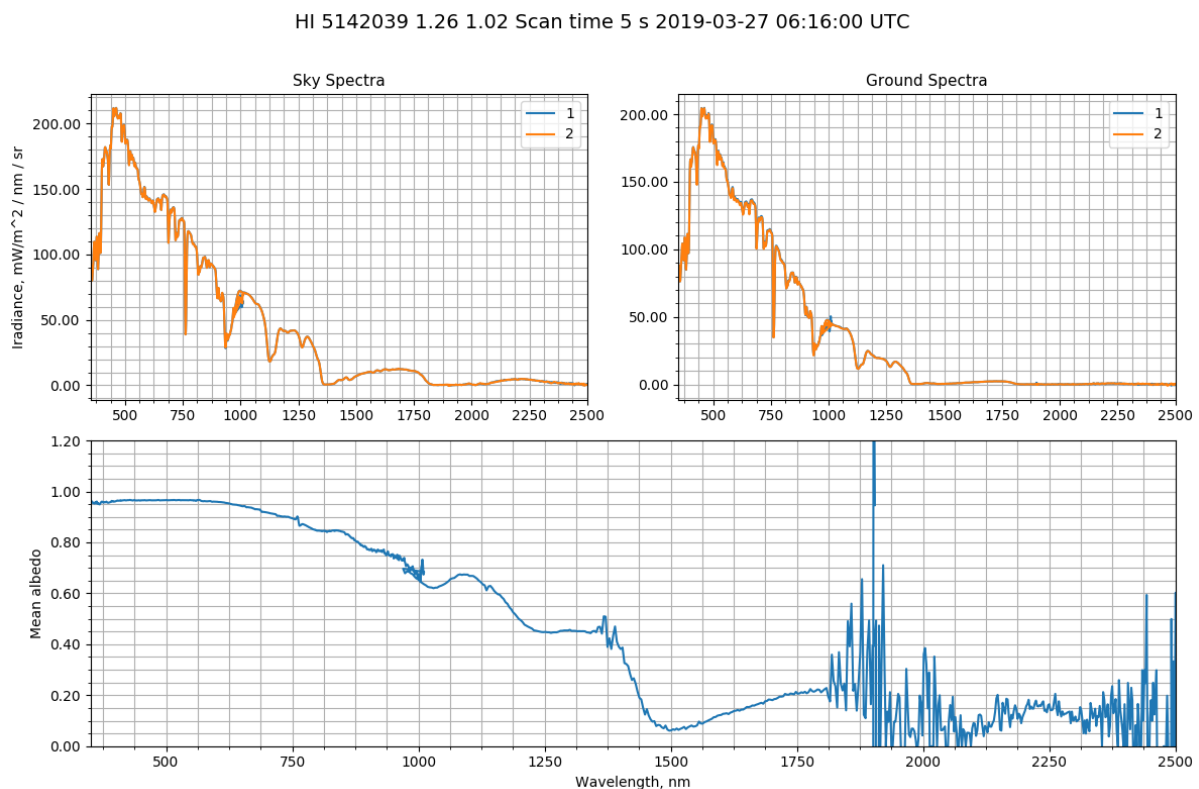


*Figure 19: Example of spectra measured by the SVC-FMI spectro-albedometer on the 27 March 2019 at 6:18 UTC.*

### ***Spectrum of surface albedo***

Ancillary data is needed for the calculation of the irradiance from the raw counts of photons, including e.g. integration time and temperature of each of the three photodiodes, scanning time, and the number of averaged spectra during the scanning time. Before each scan, the instrument automatically measures the dark current and

subtract it from the photon counts. For a quick check of the data, after each scan the averaged spectra of incident irradiance, reflected irradiance, and albedo are plotted (see Figure 19), and the plots are saved in a dedicated file.

The figures files, the raw data files, the ancillary data files, and the calculated irradiances and albedo files are stored in a datalogger placed inside the instrument enclosure. Data are then automatically downloaded to the receiving station or laptop via ethernet connection.

The data processing included the development of the routines to correct the data from deviation of perfect cosine response of the integrating spheres, from the thermal drift due to the temperature dependence of the sensor's sensitivity, and from the obstruction of the instrument's field of view caused by the supporting infrastructure.

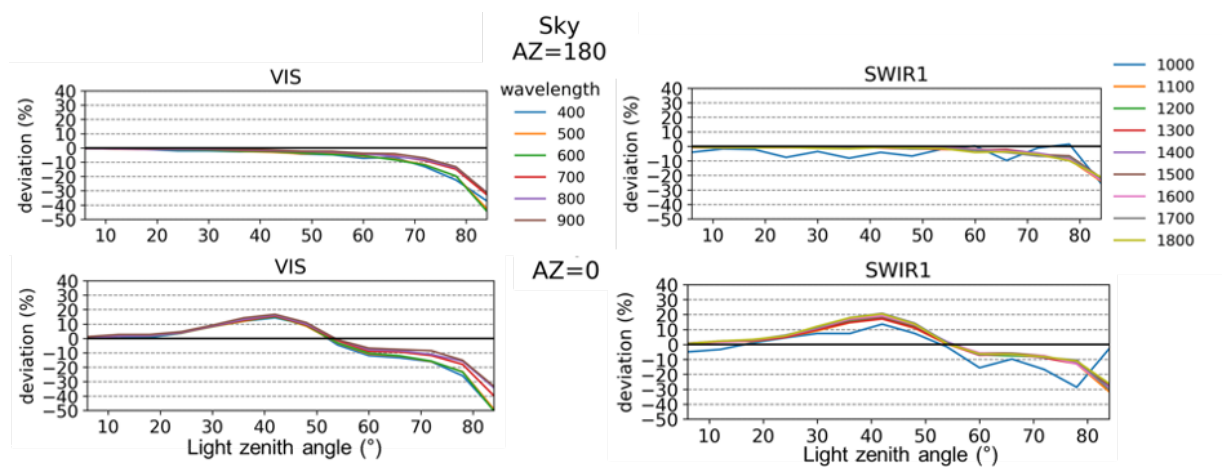


Figure 20: Deviation of the angular response of SVC-FMI spectro-albedometer from the ideal cosine response for the two sensors with the shortest wavelengths (VIS and SWIR1) and two different azimuth directions (South = 180° and North = 0°).

The non-ideal cosine response of the integrating spheres that collect the incoming and reflected light may lead to under- or overestimation of the spectral irradiances. Errors might be up to 15 % for solar zenith angles larger than 75° and are dependent on wavelength, angle of incident light, and azimuth angle. Figure 20 illustrate the angular response of the SVC-FMI spectro-albedometer measured in the FMI optical laboratory: the irradiance is underestimated at the largest zenith angles and when azimuth is close to North direction. The measured deviation was then applied to calculate the fraction of direct sunlight that has been underestimated by the spectroradiometer. This calculation required the measurement of the ratio between direct and diffuse incoming irradiance. Thus, for the automatization of the correction procedure, look up tables of the ratio between direct and diffuse incoming radiation for different solar zenith angles and for different values of the measured irradiance need to be generated via radiative transfer modelling.

Two of the three photodetectors of the SVC spectro-albedometer (measuring in the 1000 – 2500nm range) are thermally stabilized, while the visible photodiode is not. The thermal drift of the sensitivity of the visible photodiode is wavelength dependent and was measured in the FMI optical laboratory by placing the instrument inside a thermally

controlled chamber. The chamber has a quartz window that enables the instrument to measure the light coming from a lamp placed outside the chamber.

The observed drift in the ambient temperature range between  $-5\text{ }^{\circ}\text{C}$  and  $+30\text{ }^{\circ}\text{C}$  (covering the corresponding photodiode temperatures logged in winter field conditions) was very small. Considering that the enclosure of the instrument includes a thermistor to raise the internal temperature when it drops below  $+10\text{ }^{\circ}\text{C}$ , and a ventilation system to prevent overheating, the effective range of temperature variability is modest, and drift in sensitivity was corrected applying wavelength specific linear equations as functions of instrument temperature.

The structure supporting the instrument causes shadows, obstructs the field of view of the downward looking sphere, and blocks part of the incident light from reaching the surface. These effects were estimated utilizing the approach developed by (Hudson, 2010): the surface is divided into a grid of points, and for each point the angular sector from where the incident light is blocked is calculated (Figure 21a). The same is done for the viewing angles of the instrument (Figure 21b). Shadows are estimated applying a schematic representation of the supporting structure (Figure 21c). With the assumptions that all light is either entirely diffuse or perfectly direct, that all parts of the setup are black, that snow is a Lambertian reflector, and that the correction is equal at all wavelengths, we obtain an upper limit for the error, that is corrected in the processed data.

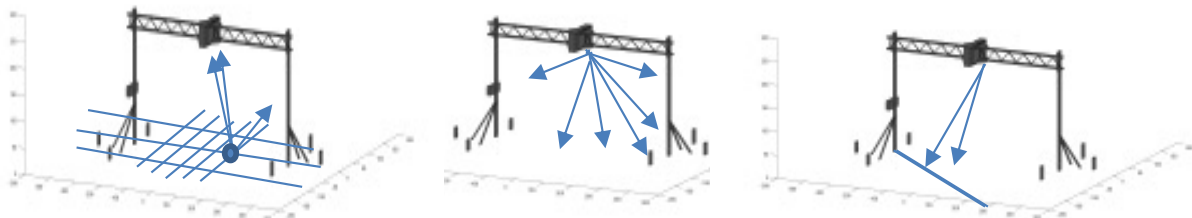


*Figure 21: The snow surface is divided into point grid, each of them scattering light in all directions (a). The obstruction of the field of view (b) and the impact of shadows (c) are estimated integrating the scatterings that the instrument receives from each point, utilizing a schematic representation of the support structure.*

#### **2.6.4. Accessibility of the obtained data sets and repositories used**

The SodScat radar data are currently available on demand for scientific use from FMI. Direct dissemination (via web portal etc.) is not encouraged due to the complexity of the dataset.

The SVC-FMI spectro-albedometer data will be published and stored in the newly developed FMI data repository (<http://fmi.b2share.csc.fi>) and, after the first peer reviewed article describing the instrument and measurement routine will be published (expected submission by end of 2021), the data will be made openly accessible also from the FMI Arctic Space Centre.

#### **2.6.5. Future plans for operation of the observing system, including data provision**

##### ***SodScat scatterometer***



Operational measurements with SodScat, running in SAR mode, have been ongoing since October 2019. The present plan is to collect multi-year timeseries with the baseline acquisition mode (four bands, two polarizations), while allowing for dedicated campaign periods as required by various research projects. During these campaign periods, the observed frequency bands, polarization and temporal resolution can be altered as required.

### ***SVC-FMI spectro-albedometer***

The SVC-FMI spectro-albedometer is installed in a permanent support structure, enabling fast deployment and removal of the instrument. To best preserve the instrument, it will be removed in November, when there is insufficient solar radiation for meaningful measurements, and installed back in March. The data acquisition and storage systems are already automatized. The automatization of the data processing is partly completed (correction for the thermal drift, obstructions of the field of view), but the correction for the angular response still needs some refinement and we expect to complete it by the end of the project. This complete operationalization will provide a unique dataset of ready-to-use spectra of irradiance and albedo that have already been requested by ECMWF and remote sensing scientists.

## **2.7. MISU**

Atmospheric observations in the central Arctic Ocean are few, and information on the vertical structure of the atmosphere and on clouds are extremely rare, essentially limited to a few icebreaker-based expeditions. Only two reasonably complete datasets of climate processes over a full annual cycle exist, from SHEBA 1997 – 98 (Uttal et al., 2002) and more recently MOSAiC 2018 – 19 (<https://mosaic-expedition.org/>); some data for a partial year is also available from the Norwegian Young ice experiment 2015 (N-ICE2015, Granskog et al., 2016). Most data have been collected during summer expeditions, when icebreaking is comparatively easy, e.g. the Arctic Ocean Experiment 2001 (AOE-2001, Tjernström et al., 2004), the Arctic Summer Cloud-Ocean Study in 2008 (Tjernström et al., 2014), the Arctic Clouds in Summer Experiment in 2014 (ACSE, Sotiropoulou et al., 2016), the Arctic Ocean 2018 (AO2018, Vüllers et al., 2021), ALOUD and PASCAL (Knudsen et al., 2018) and Sea State (Thomson et al., 2018). There is an abundance of satellite observations over both poles of the Earth, due to converging polar-orbiting satellite tracks, but while the information may be sufficient for monitoring (Sedlar and Tjernstrom, 2019), it is insufficient for both numerical weather prediction, at least in the absence of any in-situ traditional data (e.g. Naakka et al., 2019) and for process understanding (Sedlar and Tjernstrom, 2019). Consequently, there is an urgent need to obtain more detailed research-quality information from the Arctic.

During expeditions, especially in the late 1990's and early 2000's, many of the instruments deployed were prototypes or specially designed for purpose, requiring constant oversight by dedicated engineers. Hence a full deployment typically called for a staff of 5 – 10 persons. While icebreaker-based science expeditions are somewhat frequent, one of the largest limitations for deploying advanced atmospheric observations,

besides a limited number of expeditions, becomes the limited number of berths on research icebreakers at each instance. Each expedition has a specific scientific target and while overall resources are limited, targeted atmospheric missions are only possible typically once every 5 – 10 years. Not only is this much too seldom to detect any trends; combined with the very large number of degrees of freedom of the atmosphere, the total accumulated time leads to severe under-sampling, even if the climate did not change; the climate change in the Arctic is the fastest on Earth.

However, sensor development since the start of the 21st century has been fast and many of the aforementioned instrument types have been developed into stand-alone instruments designed for unattended deployment. The vibrating and moving environment on an icebreaker navigating in thick sea ice makes this somewhat more complicated than on land, but this has opened possibilities to build an atmospheric observatory – essentially a so-called “supersite” – on an icebreaker and run it unattended or with a minimum staff. This allows deployment on all expeditions with that vessel, regardless of the science focus of individual expeditions. This concept was hatched by the *Arctic Climate Across Scales* (ACAS) project, funded by the Knut and Alice Wallenberg Foundation, roughly simultaneously with INTAROS; while most of the instrument costs were covered by ACAS, INTAROS contributed to the engineering and its first deployment. The concept is built around the Swedish research icebreaker *Oden*, owned by the Swedish Maritime Administration and chartered by the Swedish Polar Research Secretariat (SPRS) for summer expedition; assistance from the SPRS has been instrumental in developing this concept.

### **2.7.1. Results of the final implementation of the observing system**

The system described here was first deployed in 2018, while a partial unattended deployment was carried out in 2019 on the so-called Ryder expedition, to the Ryder fjord and glacier on northwest Greenland. The whole system would have been deployed again in 2020 on the Synoptic Arctic Survey, that was unfortunately cancelled due to the Covid-19 pandemic and rescheduled for summer of 2021. The system consists of several linked parts:

1. An advanced weather station (Figure 22) that, in addition to standard meteorological variables such as atmospheric pressure, wind speed and direction, air temperature and moisture, also samples incoming broadband shortwave and longwave radiation and surface temperature by infrared thermometers looking down at the surface. This set of sensors is complemented by a so-called “present weather” sensor, providing precipitation (type and intensity) and visibility, and a laser ceilometer, providing cloud-base geometry scenes and lidar backscatter intensity. These instruments are all mounted at *Oden*’s 7<sup>th</sup> deck, on the bridge roof, at ~25 meters above the surface.



Figure 22: Front view of icebreaker Oden's superstructure indicating the locations of the instruments integrated in the advanced weather station. Left inserts show the present weather sensor, the ceilometer and the infrared thermometers for surface temperature and to the right the regular weather station with the broadband radiation sensors and the location of the radiosonde station.

2. A system for vertical soundings of temperature, atmospheric water vapor, winds and pressure on free-flying helium balloons, frequently referred to as radiosoundings. The receiver station is located in a laboratory container on the 7<sup>th</sup> deck, while radiosonde launches are performed from the helipad of Oden (Figure 23). Results from each sounding, typically every 6 or 12 hours, depending on availability of staff, is shared by satellite link to the Global Telecommunications System (GTS) in near-real time making it available globally for national weather services, for forecasting and reanalysis.



Figure 23: Radiosonde launch from Oden's helicopter deck.

3. A surface turbulence flux station with instruments for eddy-covariance mounted in a special foremast of Oden (Figure 24). The instruments consist of a heated sonic anemometer collocated with an open-path gas analyzer for atmospheric water vapor (and complementary carbon dioxide) and an inertial motion sensor for correction of measured winds for ship motion at the top of the mast at ~20 m above the surface. This setup has also on a few expeditions been co-located with an inlet for a closed-path cavity-enhanced laser spectrometer for eddy-covariance observations of carbon dioxide and methane; to our knowledge the only such eddy-covariance observations existing in the Arctic.

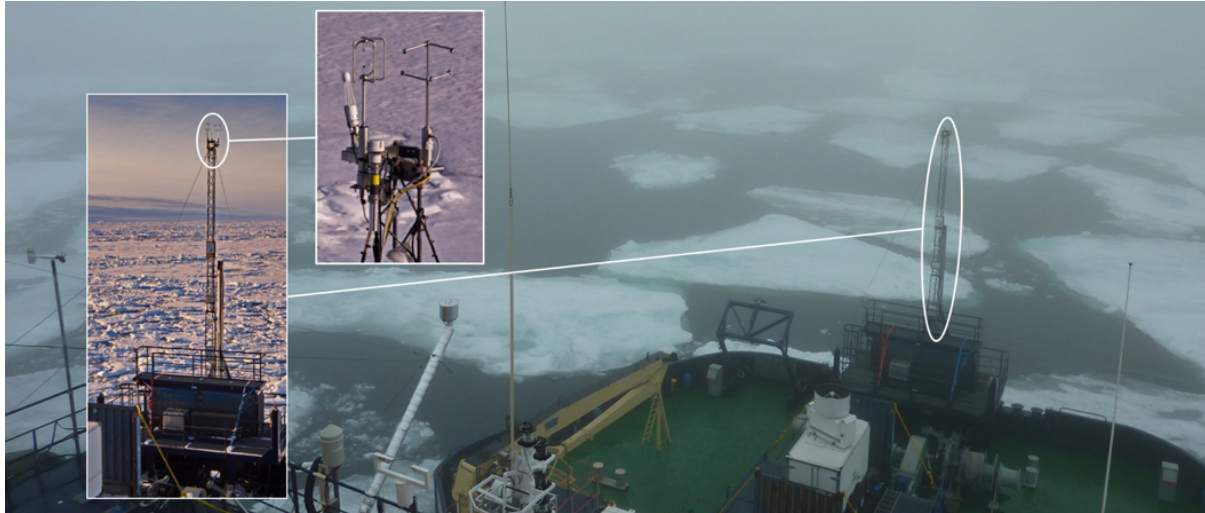


*Figure 24: Photo of Oden's foredeck a foggy day, showing the foredeck mast, with inserts of the mast on a clearer day and of the instruments at the top of the mast. Note that the photos show an earlier version of the mast installation where the instruments were accessible by a lift; today the platform is extended to the aft, from the mast to the roof of Oden's permanent foredeck lab, and the mast folds backwards hydraulically on this platform.*

4. A set of surface-based remote sensing instruments consisting of a W-Band Frequency Modulated Continuous Wave (FMCW) cloud radar and a scanning multi-frequency microwave radiometer (Figure 25). The cloud radar provides the geometry of clouds (cloud boundaries) and precipitation (radar reflectivity) and also microphysics (hydrometeor mean Doppler fall velocity and its spread) while the microwave radiometer provides vertically integrated cloud liquid water and water vapor as well as high-temporal resolution vertical profiles of temperature and water vapor, and also (although with lower quality) cloud liquid water content. Combined with the soundings and the laser ceilometer, this set of instruments provide for input to the Cloudnet algorithm (Illingworth et al., 2007).

All the systems are logged over the ship's intranet on a separate and secure virtual network, and backup storage are done on two separate raid systems located at separate locations onboard. Power supply for each system are over separate UPS systems.

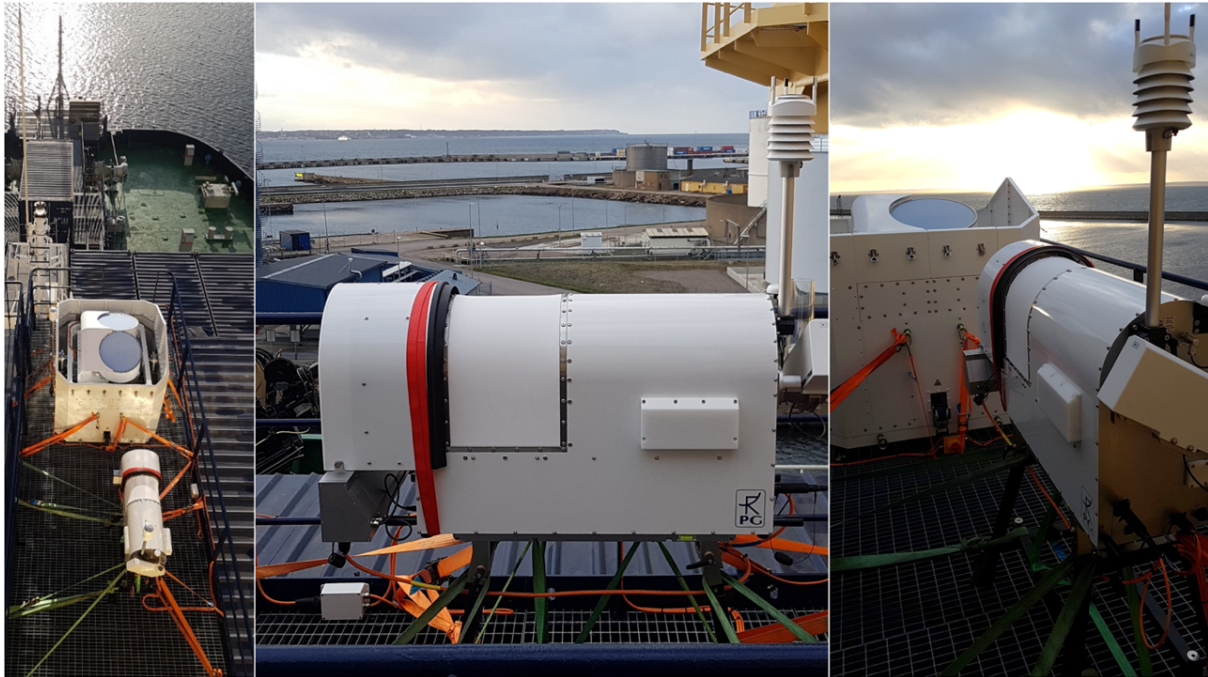


Figure 25: Surface based atmospheric remote sensing system installed on top of 4th deck mid-ship's lab container, showing (left) a top view of FMCW Doppler radar in the front of the microwave radiometer (also see the foredeck mast with the extended platform), (middle) side view from the port side of the microwave scanning radiometer (scanning to the port side) and (right) close up view of both instruments.

### 2.7.2. Lessons learned and technology challenges identified during the project

Deploying a permanent advanced observing system on an icebreaker is in many ways easier than deploying a temporary system with the same specifications. It necessitates an agreement with the owner/operator of the ship and once this is achieved, it lies in everyone's interest that the installation is robust and sustainable; no rash compromises in the interest of saving time. As an example, the foredeck mast (a development of that in Figure 24; see Figure 25) now folds backwards hydraulically for easy access to the instruments, on to a new platform that connects the mast platform with the lab container installations on the roof of the permanent foredeck lab. This installation is an example of an initiative taken by the SPRS and the ship's owner to simplify operations, that did not require any research funding. The installation of the electronics and computers for the remote sensing equipment (Figure 25) in permanent computer racks in the container below the instruments, the installation of the instruments on a permanent flat rack and the virtual isolated network on the ship's research intranet for data logging and storage are other examples where improved infrastructure has been supplied by the SPRS free of charge to the research project.

None of the installed instruments are "rocket science"; all instruments are bought off the shelf in the sense there are manufacturers of standard hardware available, although the more sophisticated remote sensing instruments were built to order. In particular, the motion stabilized platform for the radar was engineered for this application but also provided to a few other customers. The advanced weather and the eddy-covariance stations including the data logging were put together in house.

Operations in the Arctic are challenging and some problems remain, such as the ever-present icing. Especially the radiation instruments on the weather station and the open-path gas analyzer tend to form ice on the optical surfaces that need to be removed by hand; else it is recommended that instruments that can be electrically heated are artificially warmed if they do not provide sufficient internal heating from the electronics.

Two main gaps remain in the current installation; a proper research lidar and continuous wind profiling. Preferably a 3D-scanning Doppler lidar would be a powerful addition to the remote sensing suite as would a wind profiler. In place of a proper research lidar, that simply turned out to be too expensive, we are using the lidar backscatter from the ceilometer, which works reasonably well, but as a consequence we do not have any means to continuously observe the vertical profiles of the horizontal wind. Apart from several wind sensors at various locations on the ship, our only way to measure winds is by the radiosoundings, which lack temporal resolution.

Also, in contrast to the rest of the systems, that only require occasional manual intervention (i.e. cleaning off frost), the radiosoundings are labor intensive and a 6-hourly sounding schedule require > 1 dedicated staff. Inflating and releasing the balloons is currently done in the open; although we have built a balloon filling station protected from the wind in most cases, this work may still be awkward in cold and stormy conditions.

### **2.7.3. Description of processing and analysis of the obtained data**

Measurements taken on a moving ship require a careful data quality review, with different complications depending on instrument and required data product. While air temperature and humidity in summer is marginally sensitive to the heating from the ship's superstructure, that may become a much more significant problem if deployed in winter. Also, due to the superstructure, there is no perfect location anywhere on board to measure the wind. The different measurement systems therefore require different, complicated and involved preparations before the data can be released to the public.

1. For the weather station, the temperature and the relative humidity is used without any systematic corrections; a simple cleanup procedure is used where values are compared to other observations from other sensors onboard and spikes and obviously erroneous values are flagged. The winds are severely affected by the flow distortion around the ship. Essentially, only winds from  $\pm 60^\circ$  from the bow can be used and they still require a semi-empirical correction for flow distortion. For this purpose, we have performed a computational fluid dynamics simulation of the flow around the ship (Moat et al., 2015) to determine both source heights for the flow streamlines and effects on the local wind speed. An example from such a simulation is shown in Figure 26; see more below. The ship's main tower structure and the containers on the 7<sup>th</sup> deck (see Figure 22) also potentially casts shadows on the radiation sensors. For the always diffuse longwave radiation this is less of a problem but for the solar shortwave radiation this becomes a problem in optically clear conditions (cloud free or thin clouds). Therefore, the 7<sup>th</sup> deck equipment was carefully mapped with respect to angles and heights. Knowing the time of day and the position and heading of the ship, potential risks for shading can be assessed and suspicious

values flagged. With optically thick clouds present this is a smaller problem, since the radiation is then diffuse; this is assessed using the net longwave radiation, estimated from the incoming longwave radiation and the black-body radiation from the surface using the corrected surface temperature; the liquid water path from the microwave radiometer is also used for this purpose. If radiosoundings are available, we also calculate the theoretical clear sky radiation using a radiative transfer code to aid in the assessment of the radiation measurements. All weather station data are sampled at 1 Hz and averaged to 1-minute and 30-minute averages. Variables from the ceilometer (cloud bases, cloud scenes and lidar backscatter) and the present weather sensor (visibility, precipitation intensity) are provided as presented by the manufacturers standard and also averaged to 1 and 30 minutes.

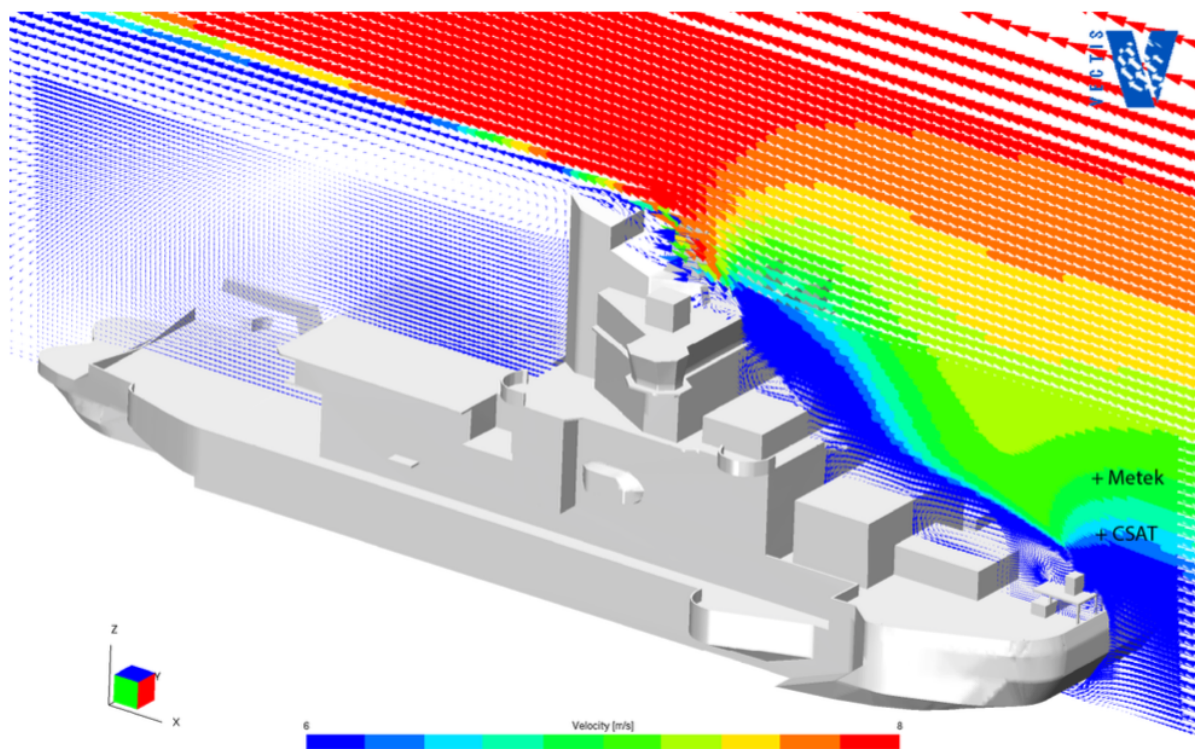


Figure 26: Example of flow distortion calculation for Oden (see Moat et al. 2015), for an on-bow wind direction and 8 m/s free stream flow. Note the wind speed reductions both at the eddy-covariance (marked “Metek”) and weather station locations as well as the wake in the lee of the superstructure.

2. For the eddy-covariance turbulent surface fluxes, a standard 30-minute averaging period is used. 3D winds are sampled at 20 Hz from the sonic anemometer and, first, corrected for ships attitude and motion using the motion-sensing data from the instrument and then combined with sonic temperature, and water vapor and CO<sub>2</sub> from the gas analyzer. Vertical fluxes and variances of momentum, sensible and latent heat and of CO<sub>2</sub> are then calculated for each 30-minute period. The exposed mast location means that, following flow distortion correction, winds  $\pm 120^\circ$  of the bow can be used. Flux coefficients are based on the mean conditions corrected for the flow distortion, given the measured wind direction and speed relative to the ship’s orientation; Figure 27 shows examples for the carbon dioxide flux as a function of wind speed and sea-ice cover from a previous expedition (Prytherch et al., 2017).

Combining all the measured energy fluxes with the weather station, surface albedo analyzed from images of the surface and the turbulent fluxes it is possible to measure the total energy budget for the surface (Figure 28).

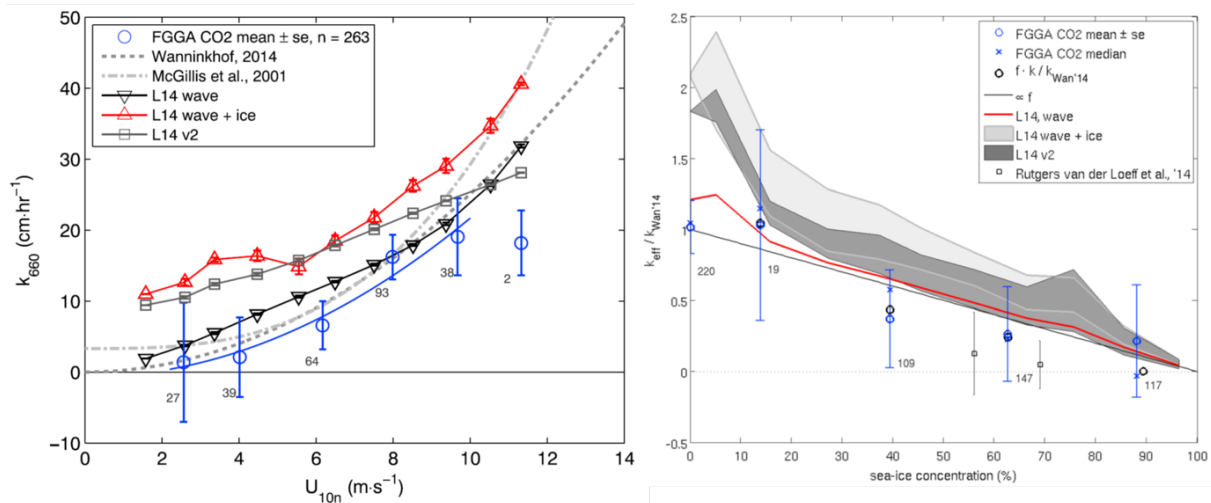


Figure 27: Examples of surface fluxes, showing (left) gas transfer constant for CO<sub>2</sub> for open water as a function of wind speed for the current system (blue) compared to some other data sets, and (right) gas transfer constants scaled to open water conditions as a function of sea ice concentration; see Prytherch et al. (2017) for a discussion.

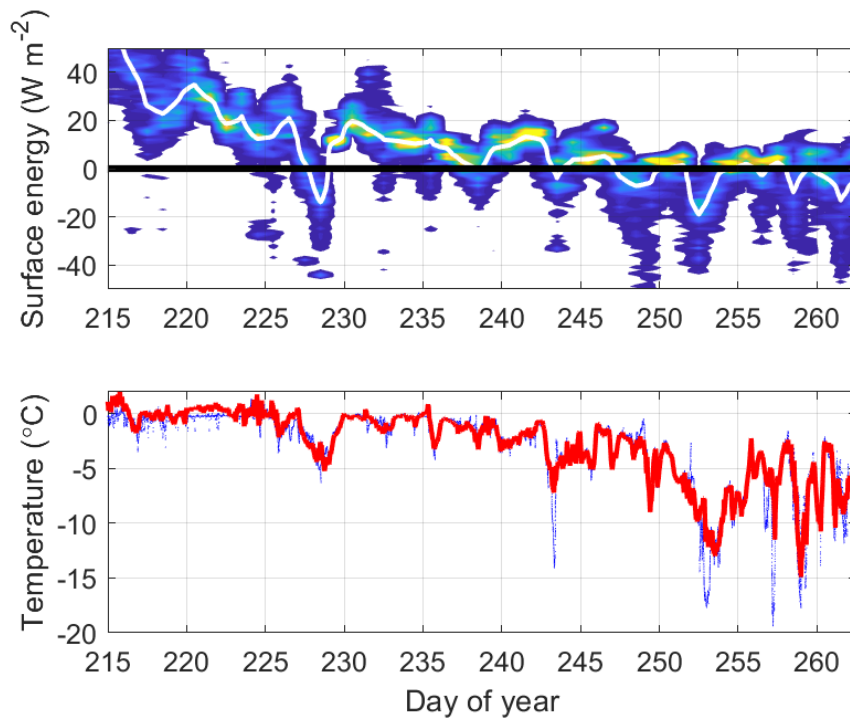


Figure 28: Time series of (upper) surface energy budget (3-hourly probability in color shading with median in solid white) and (lower) 25-meter (red) and surface (blue) temperatures, from AO2018. Note how the energy budget is positive early but with occasional dips; this is the end of the melt season when the surface temperature is stuck at the melting point. The dips are when the nearly permanent low cloud layer dissipates; also note how the surface and air temperatures immediately drop when this happens. The autumn melt is initiated around DoY240; after this day, temperatures stay well below freezing.

3. For the remote sensing data, radar and microwave radiometer data are provided in the native format for the systems as provided by the manufacturer. The Doppler



response in the radar signal is an important parameter, affected by the movements of the ship; hence the stabilized platform. But even if the radar is kept horizontal by this platform, the results still have to be corrected for the ships heave; the vertical motion of the whole platform. Hence, we have installed a separate motion sensor on the radar itself. The primary data from the radar consists of mean radar reflectivity, mean Doppler velocity and Doppler velocity spread; see example in Figure 29. For the radiometer, cloud liquid water and water vapor paths are provided as well as separate files for temperature, water vapor and cloud liquid water content profiles. Additionally, these data are combined with radiosounding profiles and lidar backscatter from the ceilometer and processed according to the Cloudnet protocol (Illingworth et al., 2007). An example of a Cloudnet product is found in Figure 30.

In terms of data products this set of instruments allows us to measure all atmospheric Essential Climate Variables (ECVs) for the surface, for the upper atmosphere (except lightning), and the energy budget of the surface; additionally, for composition, concentration and surface fluxes of CO<sub>2</sub> and sometimes CH<sub>4</sub>.

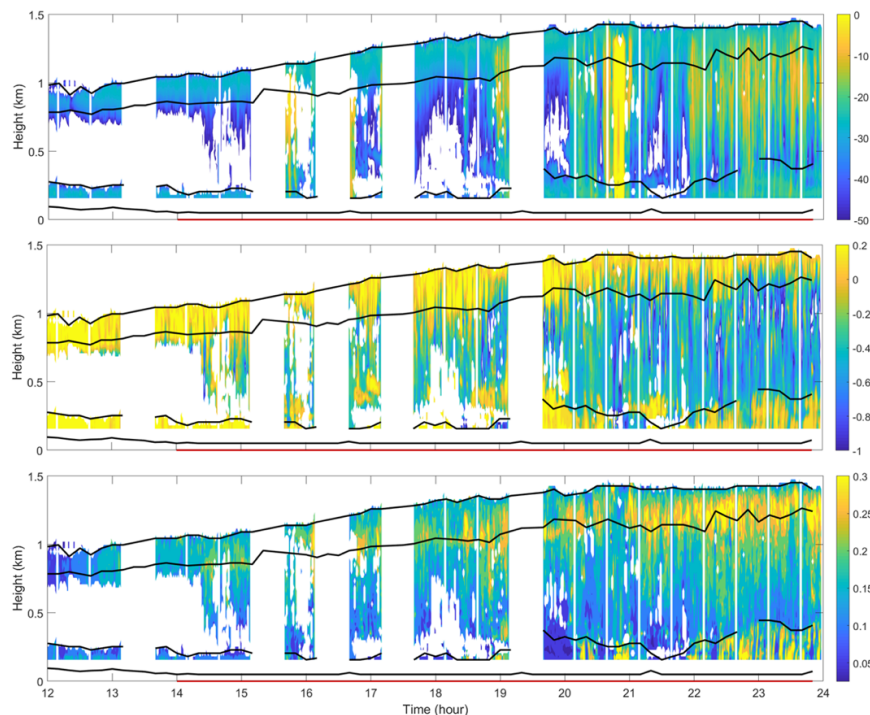


*Figure 29: Example of cloud radar data showing over a brief period 18 August during AO2018, showing (upper) radar reflectivity (dBze), (middle) mean Doppler velocity (m/s) and (lower) Doppler velocity variance (m/s). Solid lines outline an upper and a lower cloud layer; the red line indicates times with visibility < 1 km. The reflectivity indicates both cloud water and precipitation. The near-zero Doppler is from cloud droplets with a small fall velocity while the larger negative values are precipitation particles. Large values for the Doppler velocity spread appear near the upper cloud base, where non-falling cloud droplets coexist with rapidly falling precipitation particles. Precipitation starts falling already around 14-15 UTC, until around 18 UTC does not reach down to the lower cloud layer and after 20 UTC Doppler velocity spread increases also in the lower cloud layer as rapidly falling precipitation coexist with cloud droplets although the mean Doppler velocity is dominated by the latter.*

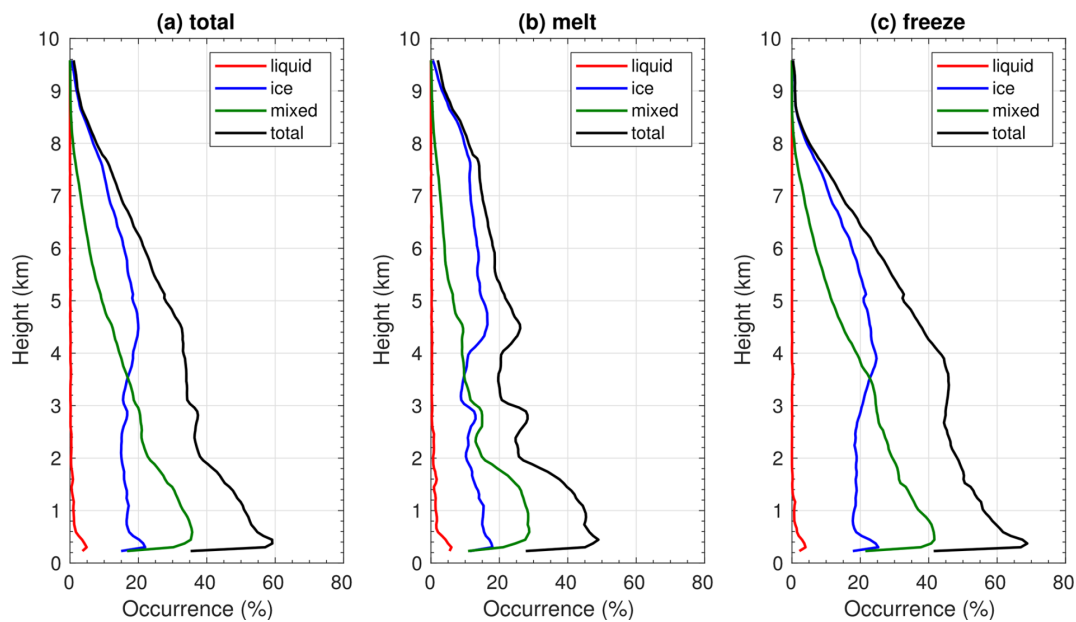


Figure 30: Examples of a Cloudnet product from Vüllers et al. (2021) showing profiles of cloud fraction divided into liquid, ice and mixed-phase clouds for the A02018 expedition, also divided into before and after onset of surface freeze, taken to occur on DoY 240 (28 August); see Figure 28.

#### 2.7.4. Accessibility of the obtained data sets and repositories used

All data will be openly available according to FAIR principles, at the Stockholm University, Bolin Centre for Climate Research database ([www.bolin.su.se/data](http://www.bolin.su.se/data)); each individual data set will be given a unique doi and can be directly downloaded.

#### 2.7.5. Future plans for operation of the observing system, including data provision

The ACAS project that originally funded most of the instrument investments is term limited and ends mid-2023. Until then we aim to deploy on all expeditions on the icebreaker *Oden* (see <https://www.polar.se/en/expeditions/timetable-for-expeditions/>).

This starts summer 2021 with the Synoptic Arctic Survey (cancelled 2020 due to the Covid-19 pandemic) and continues 2022 with the ArcOp22 ocean-floor drilling expedition. In 2023 there are two expeditions planned; ARTofMelt, initiated by ACAS to explore the onset of the summer melt and the multidisciplinary EUROASIAN Arctic C4 expedition to the Siberian shelf break to explore the Arctic carbon cycle. In 2024 there is one multidisciplinary expedition planned, to north Greenland fjords; GEOEO. The latter two expeditions and beyond will require additional funding since they occur after the end of ACAS. At that point in time a new ingestion of capital is likely needed for instrument upgrades.

### **3. Performance and fitness-to-purpose of the platforms, sensors and systems implemented during INTAROS for a future sustained Arctic observing system**

#### ***Automated flask sampler for atmospheric trace gases***

The automated flask sampler employed by MPG for sampling at remote Station North on Greenland has fulfilled all requirements for a continued operation in the Arctic. The instrument is custom-built, but can be ordered at the ICOS-FCL facility in Jena as an off-the-shelf product. Being operated by non-scientific personnel, it performed reliably and without failures over the deployment period of 21 months. Flask logistics should ideally be possible about twice per year therefore it is recommended to link this instrument to existing research sites which are regularly visited. The obtained datasets are of highest quality, and facilitate additional insights into atmospheric transport processes, and sources and sinks for trace gases, which ideally complement continuous monitoring of atmospheric trace gases using e.g. Picarro or LosGatos greenhouse gas analyzers.

#### ***Sonic anemometer de-icing***

Improving the temporal and spatial coverage of both CO<sub>2</sub> and CH<sub>4</sub> flux data and making these data accessible to the wider arctic research community will contribute to closing a critical knowledge gap in the current state of arctic carbon-climate feedback representation in models. There is considerable need for a long-term, year-round measurement program. Past efforts tended to emphasize the summer period, whereas we only recently (2013) started collecting a full suite of critical measurements year-round. A sonic anemometer with an automatically controlled de-icing system is critical in this context, and therefore also for an Arctic observing system which aims to collect long-term carbon flux measurements.

We replaced the CSAT-3BH, which was the US-manufactured heated sonic we initially planned to install in all the sites, with a METEK Class A, which proved to have a much more effective de-icing. This change was related to the problem with the de-icing of the CSAT-3BH: the heating units of the CSAT were not able to successfully de-ice the sonic during the winter. The METEK Class A is an improved version of the METEK sonic we installed in two sites in 2013 and includes a better control of the de-icing based on both quality flags and air temperature. Once installed, this system should autonomously de-ice the sonic and allow data collection without human intervention. The de-icing of the sonic requires very little maintenance, and we expect to only require minimal human intervention, therefore it is highly suitable for routine operations.

#### ***High-resolution soil temperature profiles***

A high-resolution soil temperature profile system is needed to be able to define the soil freezing and thawing processes which are critical to explain a wide range of processes, including erosion, and carbon emissions from the permafrost in the Arctic region. The high-resolution soil temperature profile systems tested by USFD were specifically designed to capture the soil freezing processes during the zero curtain (ZC), a period

when daily mean soil temperatures were between 0.75 °C and -0.75 °C. Thanks to the installation of this system, which extended the soil temperature measurements down to 1 m depth below the surface, we realize that the shallower soil depths may underestimate the duration of the ZC compared to the deeper high-resolution soil temperature profile. We protected the cables with aluminum conduit to minimize maintenance. The high-resolution profile system will allow unattended recording of soil temperature, and automated data transmission to a data repository, and is therefore highly suitable to be included in operational Arctic soil monitoring systems.

### ***The snow and soil thermal conductivity measurement system***

A novel development of the environmental monitoring in the Eastern Canadian Arctic is the monitoring of snow and soil thermal conductivity. Indeed, besides snow temperature, no vertical profiles of snow physical properties had been monitored before. This system provides a unique diagnostic for snow physics modeling, and time series of snow thermal conductivity can inform us on snow-climate feedbacks. The system, described in Domine et al. (2015), can essentially be deployed anywhere. The program to run the Campbell CR1000 data logger is fairly complex. It can be obtained from F. Domine and will be made available online. The instruments are commercially available TP08 heated needle probes from Hukseflux. Snow thermal conductivity measurements using TP08 needles is affected by a negative artefact, but a correction routine based on snow density has been developed and will hopefully appear in the literature soon (Fourteau et al., J. Glaciol., submitted in 2021).

### ***The SodScat scatterometer***

The SodScat scatterometer is a custom-built prototype of a ground-based radar suitable for operation in Arctic conditions, designed and built by Harp Technologies Ltd. (Finland) with FMI funding. During the INTAROS project, efforts were focused on upgrading the system to an operational status by means of acquiring a 3-axis pointing device, displacement rail, and developing software for remote operation of the instrument (pointing device and rail acquired using FMI internal funding). A protocol for radiometric calibration and SAR image reconstruction using time-domain back-projection was developed, enabling the fast processing of science-quality data. An integral part of the activity was also the definition of best practices for instrument operation and maintenance in Arctic conditions. SodScat data will be usable for cal/val activities of operational SAR satellite sensors as well as the development of forward models and retrieval methods of geophysical variables using SAR.

### ***The SVC-FMI spectro-albedometer***

The developed measuring system, with the weather-proof enclosure, internal heating, and ventilation of the domes to prevent frost formation has proven to withstand harsh winter conditions in the terrestrial Arctic and can be applied for continuous measurements with minimal maintenance effort. The developed instrument is therefore a viable solution for unattended measurements of the full spectrum of incoming irradiance and surface albedo. These measurements are very much needed for the development of algorithms to retrieve snow properties from satellite optical sensors, and

for the monitoring and modelling of the surface snow and sea ice albedo. This instrument is a robust and economically convenient solution compared to the traditional manually operated instruments.

### ***The MISU shipborne atmospheric “super site”***

The concept of building a super site of observations that can be operated by a few or even partly run autonomously has been proven to be viable. Open and constructive communication and collaboration between the scientists operating the system and the organization running the ship based on mutual benefits is important for success. It is also important to have continuous staff resources; this facilitates the implementation of the instruments but also data handling and management. This super site has only been tested under summer conditions but should work also in other conditions, given the opportunity of available vessels in other seasons. Some gaps remain, most notably continuous observations of vertical profiles of horizontal winds, and icing of instruments remain a problem. The investment in instruments is expensive. An installation like this is unlikely to be deployed on many ships. Still considering the cost of other instruments examining the Arctic atmosphere, for example satellites, and the almost complete lack of information on surface fluxes or atmospheric vertical structure over the Arctic Ocean, this is a worthwhile investment.

## **4. Summary**

This report summarized findings from a distributed network of novel observation techniques in the terrestrial and atmospheric spheres across the Arctic. Lacking a substantial methodological or geographic overlap, the individual activities that represent distributed terrestrial and atmospheric observations have to be evaluated separately, not as a coherent network. They have in common that they all address crucial gaps in Arctic observing capacities, and provide important steps forward towards operational solutions to improve observational networks.

All seven partners involved in this part of INTAROS successfully implemented their observation systems, and collected novel datasets in their respective fields, as described in the description of work. However, all projects were challenged by restrictions related to the COVID-19 pandemic, with more or less severe limitations to accessing research sites, carrying out experiments, and maintaining existing instrumentation: (i) some expeditions that were intended to contribute to this reporting could not be carried out; (ii) installation of new instruments, or relocation of systems, had to be postponed by one year or more, so that insights based on these upgrades are not available at the time of writing; (iii) lacking site access, datasets were lost because they could not be retrieved on time before being overwritten on the data logger. Despite these problems, each project included in this report provided valuable insights on novel approaches to fill crucial gaps in the terrestrial and atmospheric observation networks in the Arctic, including practical experience in operating these systems under harsh Arctic climate conditions, demonstration of the quality of the datasets that can be produced, and suitability of the employed systems for long-term operational monitoring.

Data from all seven projects have been made accessible in public repositories to the Arctic research community. This includes a pledge to continue uploading updated datasets in the future for those systems that will be kept operational beyond the INTAROS project period. The availability of these new datasets, which each fill important gaps in previous Arctic data coverage, certainly also benefits activities within INTAROS WP6.

## 5. Literature

Arndt, K. A., Oechel, W. C., Goodrich, J. P., Bailey, B. A., Kalhori, A., Hashemi, J., Sweeney, C., and Zona, D.: Sensitivity of Methane Emissions to Later Soil Freezing in Arctic Tundra Ecosystems, *J. Geophys. Res.-Biogeo.*, 124, 2595-2609, 2019.

Arndt, K. A., Lipson, D. A., Hashemi, J., Oechel, W. C., and Zona, D.: Snow melt stimulates ecosystem respiration in Arctic ecosystems, *Glob. Change Biol.*, 26, 5042-5051, 2020.

Domine, F., Barrere, M., Sarrazin, D., Morin, S., and Arnaud, L.: Automatic monitoring of the effective thermal conductivity of snow in a low-Arctic shrub tundra, *Cryosphere*, 9, 1265-1276, 2015.

Domine, F., Lackner, G., Sarrazin, D., Poirier, M., and Belke-Brea, M.: Meteorological, snow and soil data (2013–2019) from a herb tundra permafrost site at Bylot Island, Canadian high Arctic, for driving and testing snow and land surface models, *Earth Syst. Sci. Data Discuss.*, 2021, 1-23, 2021.

Granskog, M. A., Assmy, P., Gerland, S., Spreen, G., and Smedsrud, L. H.: Arctic research on thin ice: Consequences of Arctic sea ice loss [peer-reviewed], *EOS Transactions*, 2016.

Hartmann, J., Gehrman, M., Kohnert, K., Metzger, S., and Sachs, T.: New calibration procedures for airborne turbulence measurements and accuracy of the methane fluxes during the AirMeth campaigns, *Atmos. Meas. Tech.*, 11, 4567-4581, 2018.

Hashemi, J., Zona, D., Arndt, K. A., Kalhori, A., and Oechel, W. C.: Seasonality buffers carbon budget variability across heterogeneous landscapes in Alaskan Arctic Tundra, *Environ. Res. Lett.*, 2021.

Hudson, S.: The srhShadow Functions for Shadow Corrections in Matlab. Version 1.0, Norwegian Polar Institute, <https://tryggve.npolar.no/ftpout/Hudson/srhShadow/>, 2010.

Illingworth, A. J., Hogan, R. J., O'Connor, E. J., Bouniol, D., Brooks, M. E., Delanoe, J., Donovan, D. P., Eastment, J. D., Gaussiat, N., Goddard, J. W. F., Haeffelin, M., Baltink, H. K., Krasnov, O. A., Pelon, J., Piriou, J. M., Protat, A., Russchenberg, H. W. J., Seifert, A., Tompkins, A. M., van Zadelhoff, G. J., Vinit, F., Willen, U., Wilson, D. R., and Wrench, C. L.: Cloudnet - Continuous evaluation of cloud profiles in seven operational models using ground-based observations, *B. Am. Meteorol. Soc.*, 88, 883-+, 2007.

Knudsen, E. M., Heinold, B., Dahlke, S., Bozem, H., Crewell, S., Gorodetskaya, I. V., Heygster, G., Kunkel, D., Maturilli, M., Mech, M., Viceto, C., Rinke, A., Schmithüsen, H., Ehrlich, A., Macke, A., Lüpkes, C., and Wendisch, M.: Meteorological conditions during

the ACLOUD/PASCAL field campaign near Svalbard in early summer 2017, *Atmos. Chem. Phys.*, 18, 17995-18022, 2018.

Levin, I., Karstens, U., Eritt, M., Maier, F., Arnold, S., Rzesanke, D., Hammer, S., Ramonet, M., Vítková, G., Conil, S., Heliasz, M., Kubistin, D., and Lindauer, M.: A dedicated flask sampling strategy developed for Integrated Carbon Observation System (ICOS) stations based on CO<sub>2</sub> and CO measurements and Stochastic Time-Inverted Lagrangian Transport (STILT) footprint modelling, *Atmos. Chem. Phys.*, 20, 11161-11180, 2020.

Mauder, M., and Foken, T.: Eddy-Covariance software TK3, Zenodo, <https://doi:10.5281/zenodo.20349>, 2015.

Moat, B. I., Yelland, M. J., and Brooks, I. M.: Airflow distortion at instrument sites on the ODEN during the ACSE project, National Oceanography Centre, Southampton, UK, <http://eprints.soton.ac.uk/385311>, 2015.

Naakka, T., Nygård, T., Tjernström, M., Vihma, T., Pirazzini, R., and Brooks, I. M.: The Impact of Radiosounding Observations on Numerical Weather Prediction Analyses in the Arctic, *Geophys. Res. Lett.*, 46, 8527-8535, 2019.

Pirazzini, R., Räisänen, P., Vihma, T., Johansson, M., and Tastula, E. M.: Measurements and modelling of snow particle size and shortwave infrared albedo over a melting Antarctic ice sheet, *Cryosphere*, 9, 2357-2381, 2015.

Prytherch, J., Brooks, I. M., Crill, P. M., Thornton, B. F., Salisbury, D. J., Tjernström, M., Anderson, L. G., Geibel, M. C., and Humborg, C.: Direct determination of the air-sea CO<sub>2</sub> gas transfer velocity in Arctic sea ice regions, *Geophys. Res. Lett.*, 44, 3770-3778, 2017.

Reichstein, M., Falge, E., Baldocchi, D., Papale, D., Aubinet, M., Berbigier, P., Bernhofer, C., Buchmann, N., Gilmanov, T., Granier, A., Grünwald, T., Havrankova, K., Ilvesniemi, H., Janous, D., Knohl, A., Laurila, T., Lohila, A., Loustau, D., Matteucci, G., Meyers, T., Miglietta, F., Ourcival, J. M., Pumpanen, J., Rambal, S., Rotenberg, E., Sanz, M., Tenhunen, J., Seufert, G., Vaccari, F., Vesala, T., Yakir, D., and Valentini, R.: On the separation of net ecosystem exchange into assimilation and ecosystem respiration: review and improved algorithm, *Glob. Change Biol.*, 11, 1424-1439, 2005.

Sedlar, J., and Tjernstrom, M.: A Process-Based Climatological Evaluation of AIRS Level 3 Tropospheric Thermodynamics over the High-Latitude Arctic, *Journal of Applied Meteorology and Climatology*, 58, 1867-1886, 2019.

Sotiropoulou, G., Tjernström, M., Sedlar, J., Achtert, P., Brooks, B. J., Brooks, I. M., Persson, P. O. G., Prytherch, J., Salisbury, D. J., Shupe, M. D., Johnston, P. E., and Wolfe, D.: Atmospheric Conditions during the Arctic Clouds in Summer Experiment (ACSE): Contrasting Open Water and Sea Ice Surfaces during Melt and Freeze-Up Seasons, *J. Clim.*, 29, 8721-8744, 2016.

Thomson, J., Ackley, S., Girard-Ardhuin, F., Ardhuin, F., Babanin, A., Boutin, G., Brozena, J., Cheng, S., Collins, C., Doble, M., Fairall, C., Guest, P., Gebhardt, C., Gemrich, J., Graber, H. C., Holt, B., Lehner, S., Lund, B., Meylan, M. H., Maksym, T., Montiel, F., Perrie, W., Persson, O., Rainville, L., Erick Rogers, W., Shen, H., Shen, H., Squire, V., Stammerjohn, S., Stopa, J., Smith, M. M., Sutherland, P., and Wadhams, P.: Overview of the Arctic Sea State and Boundary Layer Physics Program, *J. Geophys. Res.-Oceans*, 123, 8674-8687, 2018.

Tjernström, M., Leck, C., Persson, P. O. G., Jensen, M. L., Oncley, S. P., and Targino, A.: The summertime Arctic atmosphere - Meteorological measurements during the Arctic Ocean experiment 2001, *B. Am. Meteorol. Soc.*, 85, 1305-1321, 2004.

Tjernström, M., Leck, C., Birch, C. E., Bottenheim, J. W., Brooks, B. J., Brooks, I. M., Backlin, L., Chang, Y. W., de Leeuw, G., Di Liberto, L., de la Rosa, S., Granath, E., Graus, M., Hansel, A., Heintzenberg, J., Held, A., Hind, A., Johnston, P., Knulst, J., Martin, M., Matrai, P. A., Mauritsen, T., Muller, M., Norris, S. J., Orellana, M. V., Orsini, D. A., Paatero, J., Persson, P. O. G., Gao, Q., Rauschenberg, C., Ristovski, Z., Sedlar, J., Shupe, M. D., Sierau, B., Sirevaag, A., Sjogren, S., Stetzer, O., Swietlicki, E., Szczodrak, M., Vaattovaara, P., Wahlberg, N., Westberg, M., and Wheeler, C. R.: The Arctic Summer Cloud Ocean Study (ASCOS): overview and experimental design, *Atmos. Chem. Phys.*, 14, 2823-2869, 2014.

Uttal, T., Curry, J. A., McPhee, M. G., Perovich, D. K., Moritz, R. E., Maslanik, J. A., Guest, P. S., Stern, H. L., Moore, J. A., Turenne, R., Heiberg, A., Serreze, M. C., Wylie, D. P., Persson, O. G., Paulson, C. A., Halle, C., Morison, J. H., Wheeler, P. A., Makshtas, A., Welch, H., Shupe, M. D., Intrieri, J. M., Stamnes, K., Lindsey, R. W., Pinkel, R., Pegau, W. S., Stanton, T. P., and Grenfeld, T. C.: Surface heat budget of the Arctic Ocean, *B. Am. Meteorol. Soc.*, 83, 255-275, 2002.

Vüllers, J., Achtert, P., Brooks, I. M., Tjernström, M., Prytherch, J., Burzik, A., and Neely Iii, R.: Meteorological and cloud conditions during the Arctic Ocean 2018 expedition, *Atmos. Chem. Phys.*, 21, 289-314, 2021.

----- END of DOCUMENT-----





# INTAROS

This report is made under the project  
**Integrated Arctic Observation System (INTAROS)**  
 funded by the European Commission Horizon 2020 program  
 Grant Agreement no. 727890.

## Project partners:

